Part IV

Convection in solid shells with solid–liquid phase change at the boundary

Solid–liquid interfaces in planetary sciences

- Convection in planetary mantles interacting with a liquid layer above and/or below. Applies to:
  - magma ocean above the mantle during its crystallisation ($\sim 10\mathrm{Ma}$).
  - Basal magma ocean for a longer period (few Gyr, Labrosse et al, 2007).
  - Icy satellites with a buried ocean below one or between two possibly convecting ice layers.
  - The inner core of terrestrial planets.

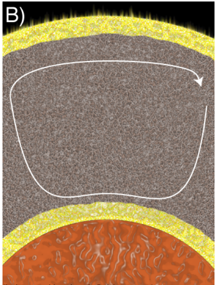

(Labrosse, Hernlund, Coltice, 2007)

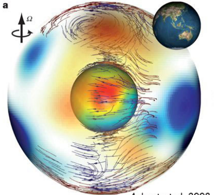

Aubert et al, 2008

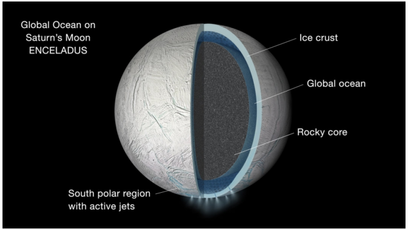

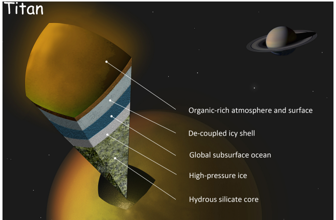

(image modified from A Taviani)

Outline

We consider a solid that behaves like a very viscous fluid on long time-scales $\Rightarrow$ Infinite Prandtl number.

$$\boldsymbol{\nabla} \cdot \boldsymbol{u} = 0 \tag{1}$$

$$-\boldsymbol{\nabla} p + \nabla^2 \boldsymbol{u} + Ra\, T \boldsymbol{e}_z = 0 \tag{2}$$

$$\frac{\partial T}{\partial t} + \boldsymbol{u} \cdot \boldsymbol{\nabla} T = \nabla^2 T \tag{3}$$

Usual boundary conditions:

- Imposed temperature owing to efficient mixing in adjacent domain (atmosphere, ocean, liquid core).
- Non-penetrative: $u_z = 0$ on a horizontal boundary.
- Free-slip: $\partial_z u_x = \partial_z u_y = 0$.

But in fact, flow in the solid $\Rightarrow$ dynamic topography.

Phase change boundary conditions - 1

First developed for the inner core (Deguen, Alboussière, Cardin, et al)

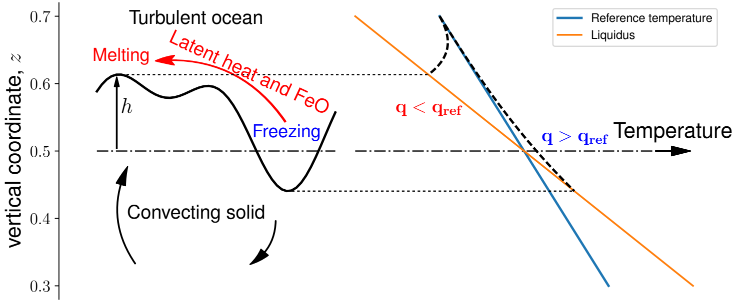

- At the boundary: continuity of the temperature:

$$T(h) = T_m(h),$$

- At the fixed computation boundary, this leads to

$$T\left(\frac{1}{2}\right) = T + \left(\frac{\partial T_m}{\partial z} - \frac{\partial T_0}{\partial z}\right) h \Rightarrow \theta\left(\frac{1}{2}\right) = \left(1 + \frac{d}{\Delta T}\frac{\partial T_m}{\partial z}\right)\frac{h}{d}.$$

- Small topography: $\theta(1/2) = 0$

First developed for the inner core (Deguen, Alboussière, Cardin, et al)

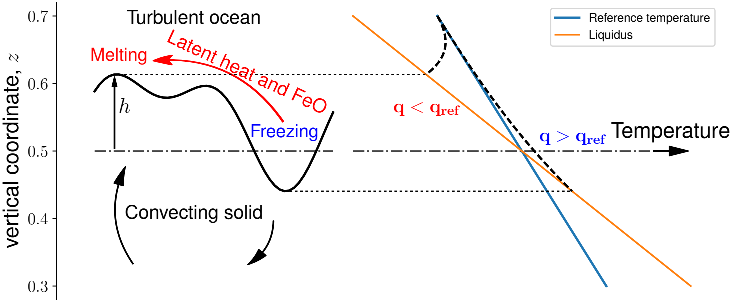

- At the boundary: continuity of the temperature:

$$T(h) = T_m(h),$$

- At the fixed computation boundary, this leads to

$$T\left(\frac{1}{2}\right) = T + \left(\frac{\partial T_m}{\partial z} - \frac{\partial T_0}{\partial z}\right) h \Rightarrow \theta\left(\frac{1}{2}\right) = \left(1 + \frac{d}{\Delta T}\frac{\partial T_m}{\partial z}\right)\frac{h}{d}.$$

- Small topography: $\theta(1/2) = 0$

Phase change boundary conditions - 1

First developed for the inner core (Deguen, Alboussière, Cardin, et al)

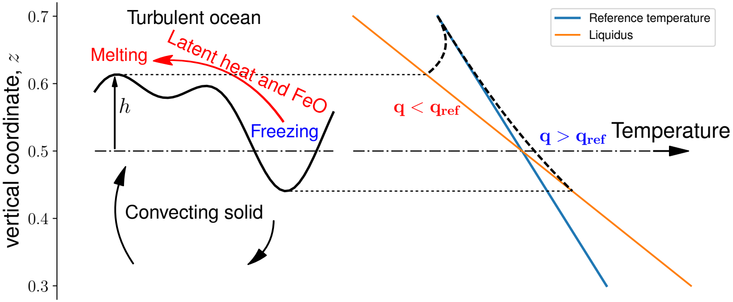

- At the boundary: continuity of the temperature:

$$T(h) = T_m(h),$$

- At the fixed computation boundary, this leads to

$$T\left(\frac{1}{2}\right) = T + \left(\frac{\partial T_m}{\partial z} - \frac{\partial T_0}{\partial z}\right) h \Rightarrow \theta\left(\frac{1}{2}\right) = \left(1 + \frac{d}{\Delta T}\frac{\partial T_m}{\partial z}\right)\frac{h}{d}.$$

- Small topography: $\theta(1/2) = 0$

Phase change boundary condition - 2

- Energy conservation across the boundary, with v_ϕ the freezing rate:

$$\rho_s L v_\phi = [\![q]\!].$$

- Assume the convective heat flow on low–viscosity liquid side, $f \sim \rho_l c_{pl} u_l \delta T_l$, dominates. Temperature variations are associated with topography so that:

$$f \sim -\rho_l c_{pl} u_l \left| \frac{\partial T_m}{\partial z} \right| h.$$

- This gives

$$\rho_s L v_\phi \sim -\rho_l c_{pl} u_l \left| \frac{\partial T_m}{\partial z} \right| h \Rightarrow v_\phi = \frac{h}{\tau_\phi}$$

with τ_ϕ the phase change time scale hence defined.

Phase change boundary condition - 2

- Energy conservation across the boundary, with v_ϕ the freezing rate:

$$\rho_s L v_\phi = [\![q]\!].$$

- Assume the convective heat flow on low–viscosity liquid side, $f \sim \rho_l c_{pl} u_l \delta T_l$, dominates. Temperature variations are associated with topography so that:

$$f \sim -\rho_l c_{pl} u_l \left| \frac{\partial T_m}{\partial z} \right| h.$$

- This gives

$$\rho_s L v_\phi \sim -\rho_l c_{pl} u_l \left| \frac{\partial T_m}{\partial z} \right| h \Rightarrow v_\phi = \frac{h}{\tau_\phi}$$

with τ_ϕ the phase change time scale hence defined.

Phase change boundary condition - 2

- Energy conservation across the boundary, with v_ϕ the freezing rate:

$$\rho_s L v_\phi = [\![q]\!].$$

- Assume the convective heat flow on low–viscosity liquid side, $f \sim \rho_l c_{pl} u_l \delta T_l$, dominates. Temperature variations are associated with topography so that:

$$f \sim -\rho_l c_{pl} u_l \left| \frac{\partial T_m}{\partial z} \right| h.$$

- This gives

$$\rho_s L v_\phi \sim -\rho_l c_{pl} u_l \left| \frac{\partial T_m}{\partial z} \right| h \Rightarrow v_\phi = \frac{h}{\tau_\phi}$$

  with τ_ϕ the phase change time scale hence defined.

Phase change boundary condition - 3

- Continuity of the vertical stress:

$$-p + 2\eta \frac{\partial w}{\partial z} + \Delta\rho g h = 0.$$

- Taking U as scale for the convective flow in the solid, this provides a scaling for the topography, $h \sim \eta U/\Delta\rho g d$ or $h = h' \eta U/\Delta\rho g d$.
- The topography evolves by phase change and viscous stress in the solid:

$$\frac{\partial h}{\partial t} = u_z + \frac{h}{\tau_\phi}$$

- Considering τ_c the time scale for the change of convective flow, using U as velocity scale, this equation is made dimensionless, with $\tau_\eta = \eta/\Delta\rho g d$:

$$\frac{\eta U}{\Delta\rho g d}\frac{1}{\tau_c}\frac{\partial h'}{\partial t'} = U u_z' + \frac{\eta U}{\Delta\rho g d}\frac{h'}{\tau_\phi} \Rightarrow \frac{\tau_\eta}{\tau_c}\frac{\partial h'}{\partial t'} = u_z' + \frac{\tau_\eta}{\tau_\phi} h'$$

- The time scale for the change of convective flow, $\tau_c \gg \tau_\eta, \tau_\phi$ and we can neglect the left–hand–side. In dimensional form, $u_z = -h/\tau_\phi$. Used in the stress–continuity equation to eliminate h.

Phase change boundary condition - 3

- Continuity of the vertical stress:

$$-p + 2\eta \frac{\partial w}{\partial z} + \Delta\rho g h = 0.$$

- Taking U as scale for the convective flow in the solid, this provides a scaling for the topography, $h \sim \eta U/\Delta\rho g d$ or $h = h'\eta U/\Delta\rho g d$.
- The topography evolves by phase change and viscous stress in the solid:

$$\frac{\partial h}{\partial t} = u_z + \frac{h}{\tau_\phi}$$

- Considering τ_c the time scale for the change of convective flow, using U as velocity scale, this equation is made dimensionless, with $\tau_\eta = \eta/\Delta\rho g d$:

$$\frac{\eta U}{\Delta\rho g d}\frac{1}{\tau_c}\frac{\partial h'}{\partial t'} = U u_z' + \frac{\eta U}{\Delta\rho g d}\frac{h'}{\tau_\phi} \Rightarrow \frac{\tau_\eta}{\tau_c}\frac{\partial h'}{\partial t'} = u_z' + \frac{\tau_\eta}{\tau_\phi}h'$$

- The time scale for the change of convective flow, $\tau_c \gg \tau_\eta, \tau_\phi$ and we can neglect the left–hand–side. In dimensional form, $u_z = -h/\tau_\phi$. Used in the stress–continuity equation to eliminate h.

Phase change boundary condition - 3

- Continuity of the vertical stress:

$$-p + 2\eta \frac{\partial w}{\partial z} + \Delta \rho g h = 0.$$

- Taking U as scale for the convective flow in the solid, this provides a scaling for the topography, $h \sim \eta U / \Delta \rho g d$ or $h = h' \eta U / \Delta \rho g d$.
- The topography evolves by phase change and viscous stress in the solid:

$$\frac{\partial h}{\partial t} = u_z + \frac{h}{\tau_\phi}$$

- Considering τ_c the time scale for the change of convective flow, using U as velocity scale, this equation is made dimensionless, with $\tau_\eta = \eta / \Delta \rho g d$:

$$\frac{\eta U}{\Delta \rho g d} \frac{1}{\tau_c} \frac{\partial h'}{\partial t'} = U u_z' + \frac{\eta U}{\Delta \rho g d} \frac{h'}{\tau_\phi} \Rightarrow \frac{\tau_\eta}{\tau_c} \frac{\partial h'}{\partial t'} = u_z' + \frac{\tau_\eta}{\tau_\phi} h'$$

- The time scale for the change of convective flow, $\tau_c \gg \tau_\eta, \tau_\phi$ and we can neglect the left–hand–side. In dimensional form, $u_z = -h/\tau_\phi$. Used in the stress–continuity equation to eliminate h.

- Continuity of the vertical stress:

$$-p + 2\eta \frac{\partial w}{\partial z} + \Delta\rho g h = 0.$$

- Taking U as scale for the convective flow in the solid, this provides a scaling for the topography, $h \sim \eta U/\Delta\rho g d$ or $h = h'\eta U/\Delta\rho g d$.
- The topography evolves by phase change and viscous stress in the solid:

$$\frac{\partial h}{\partial t} = u_z + \frac{h}{\tau_\phi}$$

- Considering τ_c the time scale for the change of convective flow, using U as velocity scale, this equation is made dimensionless, with $\tau_\eta = \eta/\Delta\rho g d$:

$$\frac{\eta U}{\Delta\rho g d}\frac{1}{\tau_c}\frac{\partial h'}{\partial t'} = U u_z' + \frac{\eta U}{\Delta\rho g d}\frac{h'}{\tau_\phi} \Rightarrow \frac{\tau_\eta}{\tau_c}\frac{\partial h'}{\partial t'} = u_z' + \frac{\tau_\eta}{\tau_\phi}h'$$

- The time scale for the change of convective flow, $\tau_c \gg \tau_\eta, \tau_\phi$ and we can neglect the left–hand–side. In dimensional form, $u_z = -h/\tau_\phi$. Used in the stress–continuity equation to eliminate h.

Phase change boundary condition - 3

- Continuity of the vertical stress:

$$-p + 2\eta \frac{\partial w}{\partial z} + \Delta\rho g h = 0.$$

- Taking U as scale for the convective flow in the solid, this provides a scaling for the topography, $h \sim \eta U/\Delta\rho g d$ or $h = h'\eta U/\Delta\rho g d$.
- The topography evolves by phase change and viscous stress in the solid:

$$\frac{\partial h}{\partial t} = u_z + \frac{h}{\tau_\phi}$$

- Considering τ_c the time scale for the change of convective flow, using U as velocity scale, this equation is made dimensionless, with $\tau_\eta = \eta/\Delta\rho g d$:

$$\frac{\eta U}{\Delta\rho g d}\frac{1}{\tau_c}\frac{\partial h'}{\partial t'} = U u'_z + \frac{\eta U}{\Delta\rho g d}\frac{h'}{\tau_\phi} \Rightarrow \frac{\tau_\eta}{\tau_c}\frac{\partial h'}{\partial t'} = u'_z + \frac{\tau_\eta}{\tau_\phi}h'$$

- The time scale for the change of convective flow, $\tau_c \gg \tau_\eta, \tau_\phi$ and we can neglect the left–hand–side. In dimensional form, $u_z = -h/\tau_\phi$. Used in the stress–continuity equation to eliminate h.

Phase change boundary conditions - 4

- The same can be done for the bottom boundary condition. Beware: the sign of $\Delta\rho$ is reversed.
- Dimensionless boundary condition for vertical velocity:

$$\pm\Phi^{\pm} w + 2\,\frac{\partial w}{\partial z} - p = 0, \qquad \text{with} \quad \Phi^{\pm} = \frac{\tau_\phi}{\tau_\eta} = \frac{\tau_{\phi^\pm}|\Delta\rho^{\pm}|gH}{\eta}$$

- $\Phi \to \infty \Rightarrow$ classical non-penetrative boundary condition $(w = 0)$.
- $\Phi \to 0 \Rightarrow$ permeable boundary condition $(w \neq 0)$.
- This boundary condition expresses the competition between the building of topography from stress in the solid and its suppression by convection in the liquid.

Outline

Plane layer with phase–change at either or both boundaries

- Linear and weakly non–linear analysis from Labrosse et al. (2018).
- Fully non–linear results from Agrusta et al. (2019).

The translation mode of convection
Labrosse et al. (2018)

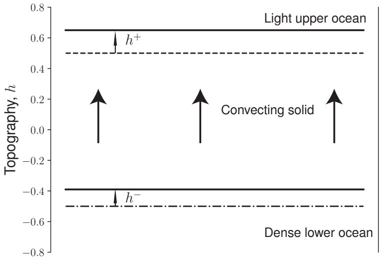

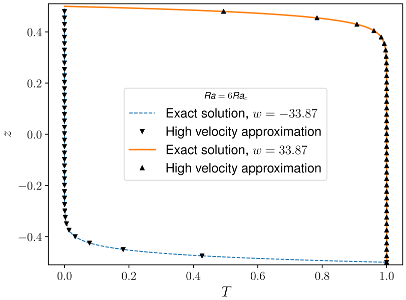

- Rigid vertical translation of the solid with continuous phase change at each boundary is possible if

$$Ra \geq Ra_c = 12\left(\Phi^+ + \Phi^-\right),$$

- In the large Rayleigh number limit ($Ra > 2Ra_c$)

$$|w| = Nu = \frac{6Ra}{Ra_c}$$

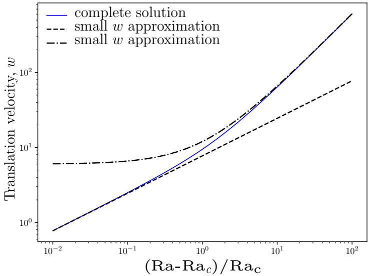

Physical interpretation

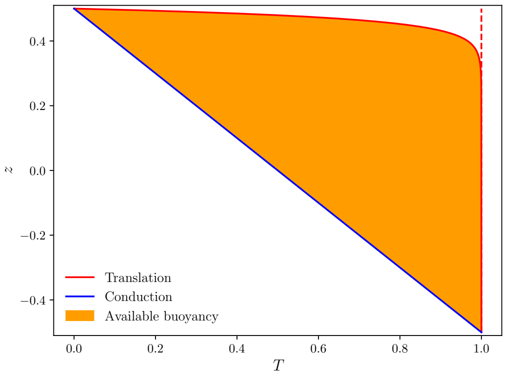

- The extra weight of the topography is balanced by the buoyancy associated with the high temperature, i.e. assuming an infinitely thin boundary layer:

$$\alpha \rho_0 g \frac{\Delta T H}{2} = \Delta \rho^+ g h^+ + \Delta \rho^- g h^-,$$

- The topography is related to the velocity by

$$h^\pm = \tau_{\phi^\pm} w.$$

- In dimensionless form:

$$w \sim \pm \frac{\mathit{Ra}}{2\left(\Phi^+ + \Phi^-\right)} = \pm \frac{6\mathit{Ra}}{R_c}$$

Linear stability for deforming modes

Find the critical Rayleigh number and the associated flow for the onset of convection as function of Φ^+ and Φ^-:

- The conservation equations for mass, momentum and temperature are linearly developed around the motionless conductive solution.
- A simple harmonic in horizontal direction:

$$\theta(x,z) = \Theta(z)\mathrm{e}^{\sigma t + \mathrm{i}kx} + c.c.; \quad w(x,z) = W(z)\mathrm{e}^{\sigma t + \mathrm{i}kx} + c.c.; \quad \text{etc.}$$

  with the wavelength $\lambda = 2\pi/k$.
- For each k, we search for the Rayleigh number $Ra(k)$ which makes $\Re(\sigma) = 0$ (neutral stability).
- The minimum of $Ra(k)$ gives the critical Rayleigh number Ra_c and the associated wavenumber k_c.
- Full calculation performed using a Chebyshev-colocation method, behaviour for small $\Phi^\pm$ obtained analytically by polynomial expansion in z and $\Phi^\pm$.

The linear operator matrix

$$
\mathbf{L} = \begin{array}{c}
\begin{array}{cccc} 0:N & 0:N & 0:N & 1:N-1 \end{array} \\
\begin{pmatrix}
\mathbf{0} & \mathrm{i}k\mathbf{I} & \mathbf{D} & \mathbf{0} \\
\mathbf{0} & \mathbf{D} & \mathrm{i}k\mathbf{I} & \mathbf{0} \\
-\mathit{Pr}\,\mathrm{i}k\mathbf{I} & \mathit{Pr}\left(\mathbf{D}^{(2)} - k^2\mathbf{I}\right) & \mathbf{0} & \mathbf{0} \\
\mathbf{0} & \mathbf{D} & \mathrm{i}k\mathbf{I} & \mathbf{0} \\
-\mathbf{I} & \mathbf{0} & \Phi^{+}\mathbf{I} + 2\mathbf{D} & \mathbf{0} \\
-\mathit{Pr}\,\mathbf{D} & \mathbf{0} & \mathit{Pr}\left(\mathbf{D}^{(2)} - k^2\mathbf{I}\right) & \mathit{Pr}\,\mathit{Ra}\,\mathbf{I} \\
-\mathbf{I} & \mathbf{0} & -\Phi^{-}\mathbf{I} + 2\mathbf{D} & \mathbf{0} \\
\mathbf{0} & \mathbf{0} & \mathbf{I} & \left(\mathbf{D}^{(2)} - k^2\mathbf{I}\right)
\end{pmatrix}
\end{array}
\begin{array}{l}
\\ 0:N \\ 0 \\ 1:N-1 \\ N \\ 0 \\ 1:N-1 \\ N \\ 1:N-1
\end{array}
$$

Convective modes at onset for $\Phi^+ = \Phi^- \equiv \Phi^\pm$

$\Phi^+ = \Phi^- = 10^5$:

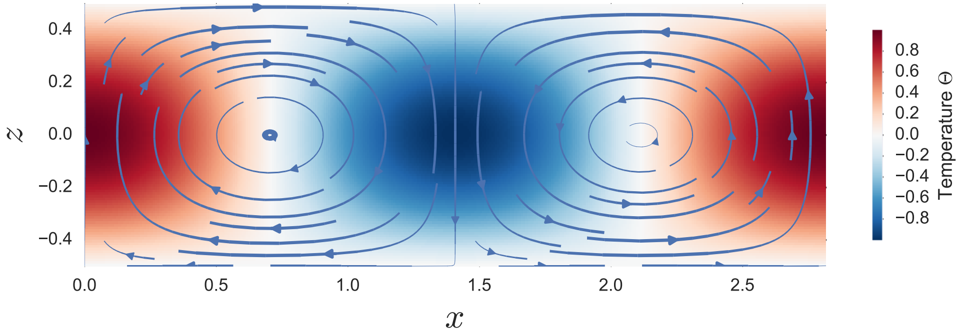

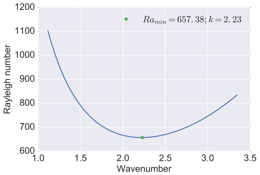

Close to Rayleigh-Bénard value for classical free-slip boundary conditions:

$$Ra_c = \frac{27\pi^4}{4}; \qquad k_c = \frac{\pi}{\sqrt{2}}$$

Convective modes at onset for $\Phi^+ = \Phi^- \equiv \Phi^\pm$

$\Phi^+ = \Phi^- = 10$:

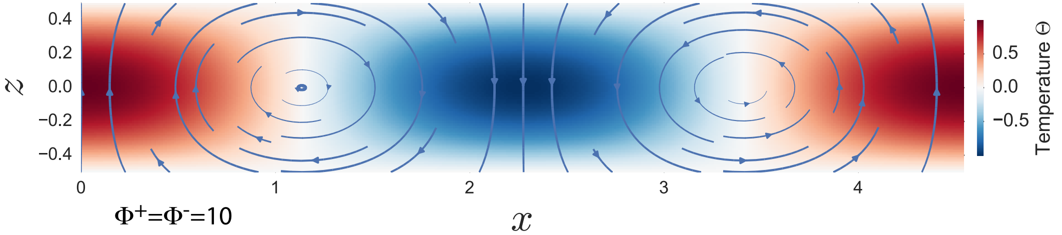

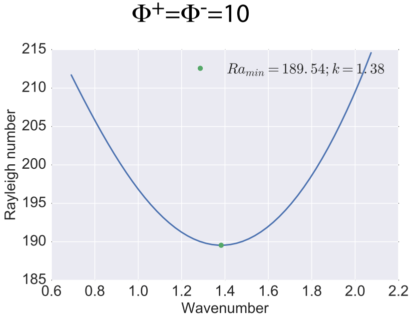

- The flow lines start to cross the boundaries.
- The wavelength gets larger and the critical Rayleigh number lower.

Convective modes at onset for $\Phi^+ = \Phi^- \equiv \Phi^\pm$

$\Phi^+ = \Phi^- = 10^{-2}$:

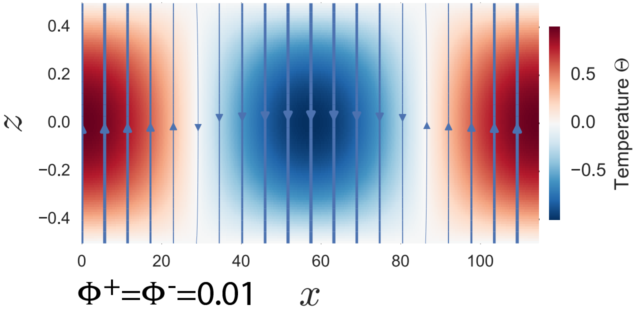

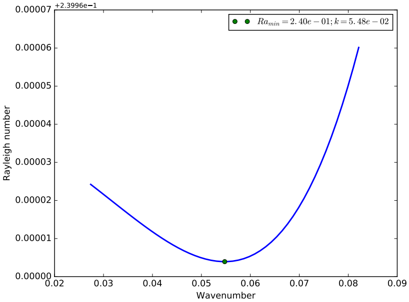

- Note the different horizontal and vertical scales here.
- The flow lines become vertical.
- The wavelength gets larger and the critical Rayleigh number lower.

Onset of convection with $\Phi^+ = \Phi^-$

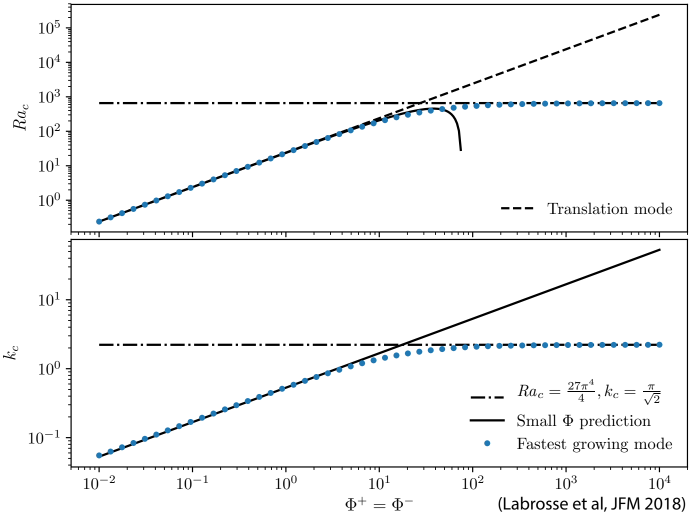

(Labrosse et al, JFM 2018)

At low $\Phi^{\pm}$, Ra_c gets close to but stays lower than that for pure translation.

Polynomial expansion of mode profiles as function of z and of the coefficients as function of Φ:

$$\Theta = \sum_{n=0}^{N} a_n z^{2n}; \quad a_n = \sum_{j=0}^{J} a_{n,j}\Phi^j; \quad Ra_c = \sum_{j=0}^{J} r_j \Phi^j, \quad k^2 = \sum_{j=0}^{J} kk_j \Phi^j.$$

Application of perturbation equations and boundary conditions at each polynomial degree leads to

$$\begin{aligned}
Ra_c &= 24\Phi - \frac{81}{256}\Phi^2; \quad k_c = \frac{3}{4\sqrt{2}}\sqrt{\phi} \\
\Theta &= (1 - 4z^2)\Theta_{max}, \\
W &= 8\Theta_{max}, \\
U &= -3\mathrm{i}\sqrt{2\Phi}\, z\Theta_{max}, \\
P &= \frac{z}{2}\left(39 - 64z^2\right)\Phi\Theta_{max}.
\end{aligned}$$

Note: the critical Rayleigh number is lower than that for pure translation.

Low Φ development II

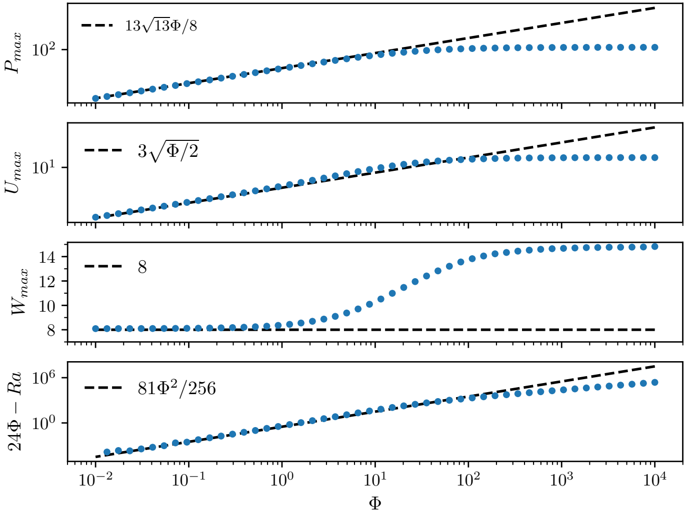

Competition between the translation mode and the deforming modes

- Translation mode is known analytically $\Rightarrow$ we can study the growth or decay of a small perturbation over it.
- For a given $\varepsilon = (Ra - Ra_c)/Ra_c$, with $Ra_c = 24\Phi$, find for which wave–numbers k the perturbation grows.

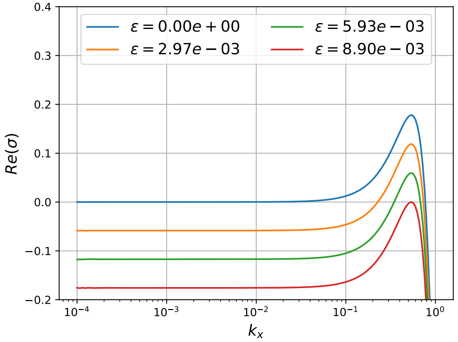

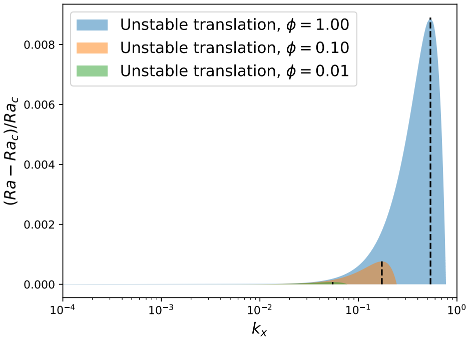

Weakly non-linear results

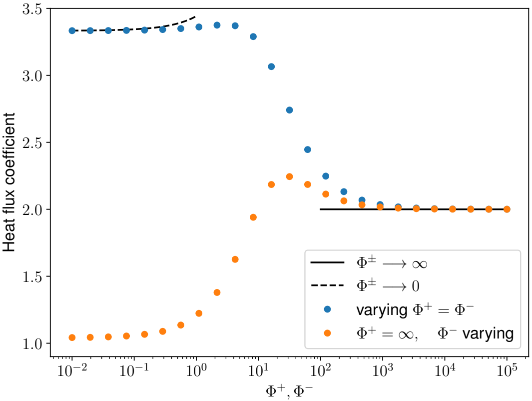

- Close to onset, the solution can be expanded as function of $Ra - Ra_c$ (Malkus & Veronis, 1958; details available on request) to get finite amplitude weakly non-linear results.
- Heat flux varies as (leading order):

$$Nu = 1 + A(\Phi^+, \Phi^-)\frac{Ra - Ra_c}{Ra_c}$$

- Classical non-penetrating boundary condition ($\Phi^+, \Phi^- \to \infty$): $A = 2$.

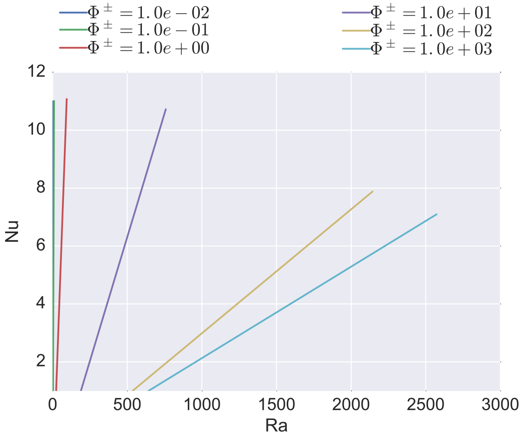

- Decreasing $\Phi^{\pm}$, the dimension-less heat flux (Nusselt number, Nu) increases:
  - because of the decrease of Ra_c.
  - because the slope $\mathrm{d}Nu/\mathrm{d}Ra$ increases to ∞ as Φ decreases to 0.

Boundary condition implemented in a finite volume code: StagYY (Tackley, 2008).

- Infinite Prandtl number convection.
- Boussinesq or Anelastic.
- Multiple geometry: 2D, 3D, cartesian, spherical, cylindrical.
- Possibility of varying physical parameters.
- Can handle variations of composition using Lagrangian tracers.

Solution structure
Agrusta et al. (2019)

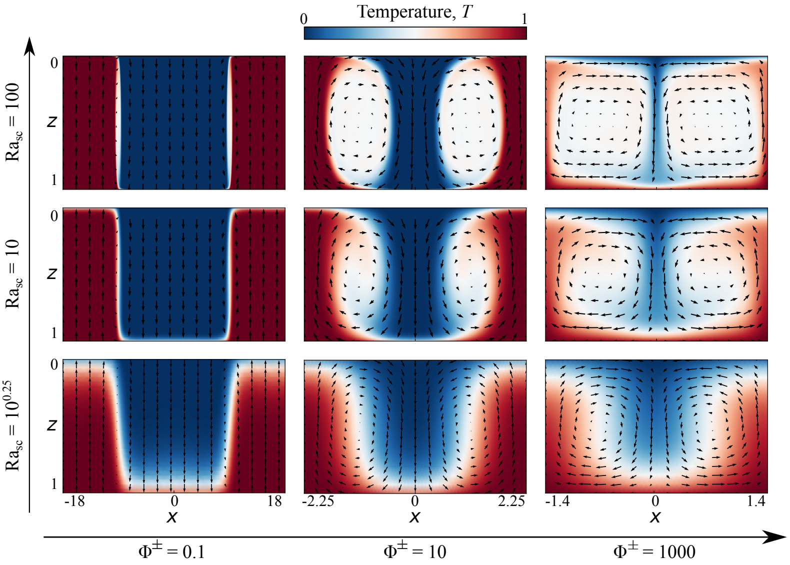

Similarity with the translation mode

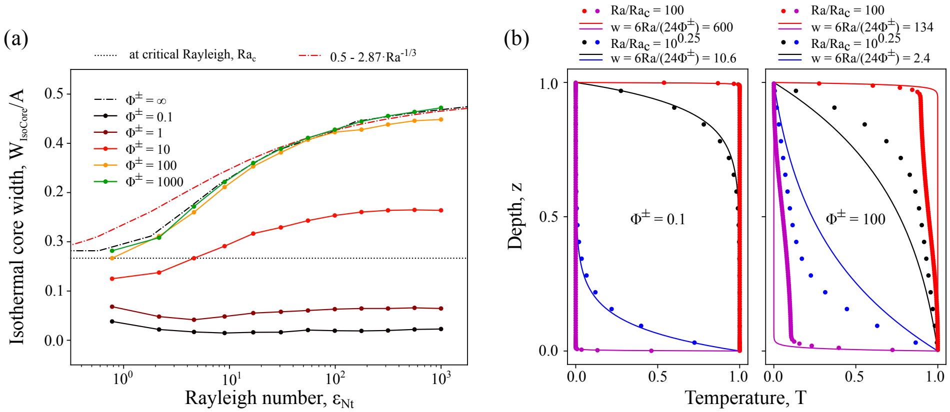

- $\Phi \leq 1$: thermal structure in each vertically moving block similar to that of the translation mode.

Heat transfer and velocity

- Dashed lines: weakly non–linear predictions to first order
- Symbols: DNS results
- Solid lines: power law fits.

- $\Phi \gg 1$: classical $Nu \sim Ra^{1/3}$
- $\Phi \lesssim 1 \Rightarrow Nu \sim Ra/\Phi$

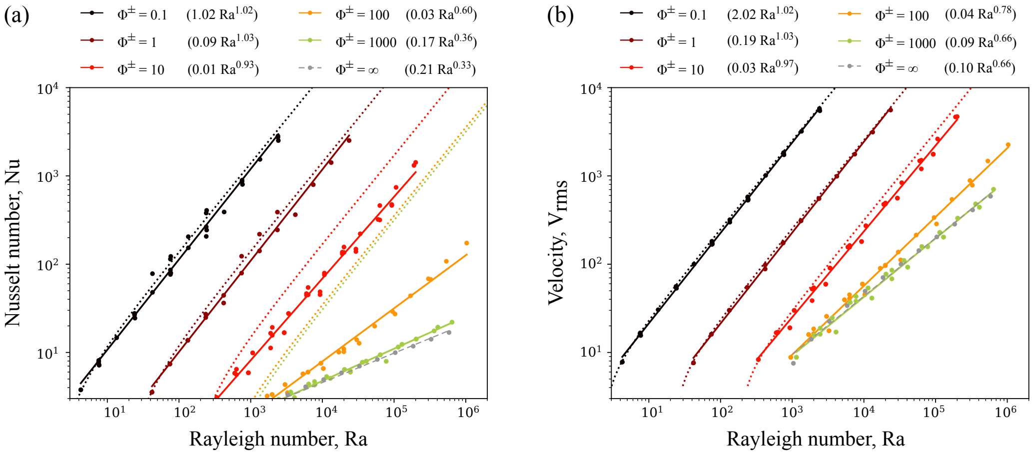

Heat transfer and velocity

- Dashed lines: weakly non–linear predictions to first order
- Symbols: DNS results
- Solid lines: power law fits.

- $\Phi \gg 1$: classical $Nu \sim Ra^{1/3}$
- $\Phi \leq 1 \Rightarrow Nu \sim Ra/\Phi$

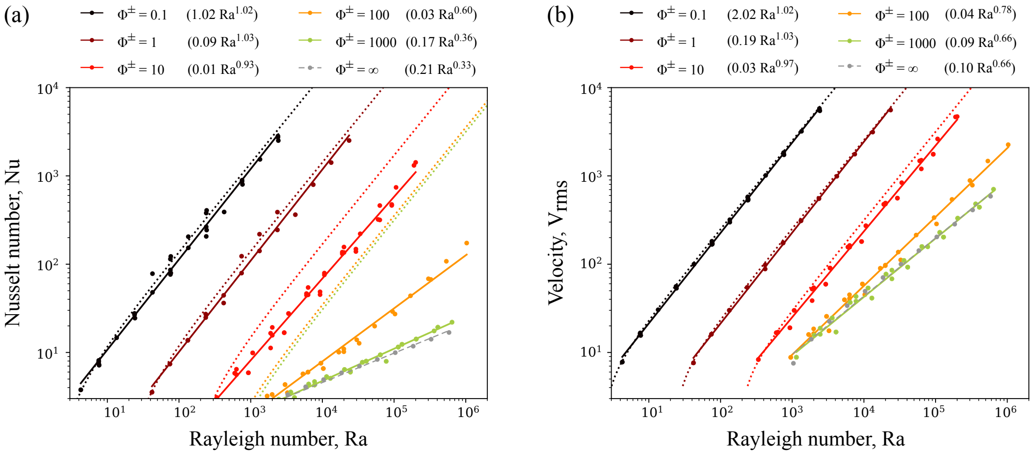

Summary on the situation with two phase change BCs

- Existence of a $k = 0$ translation mode of convection that can be solved analytically. In particular $Ra_c = 12(\Phi^+ + \Phi^-)$
- Linear stability for $k \neq 0$ shows that $Ra_c \lesssim 12(\Phi^+ + \Phi^-)$ and $k_c = 3\sqrt{\Phi}/4\sqrt{2}$.
- $k \neq 0$ solutions at low Φ composed of alternating upward and downward translating blocks quite similar to the translation mode. In particular $Nu \simeq Ra/\Phi$.
- Horizontal wavelength increases with the decrease of Φ.

Convective modes at onset as function of Φ^- ($\Phi^+ = \infty$)

$\Phi^- = 10^5$:

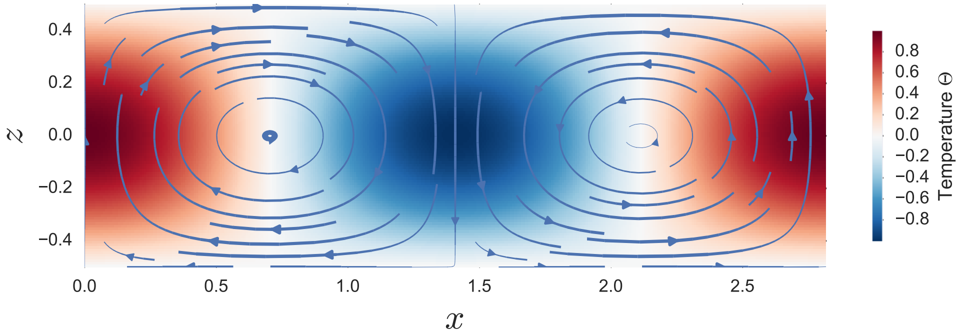

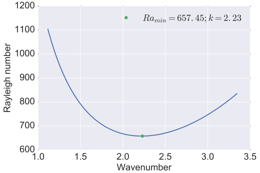

Close to Rayleigh-Bénard value for classical free-slip boundary conditions:

$$Ra_c = \frac{27\pi^4}{4}; \qquad k_c = \frac{\pi}{\sqrt{2}}$$

Convective modes at onset as function of Φ^- ($\Phi^+ = \infty$)

$\Phi^- = 10$:

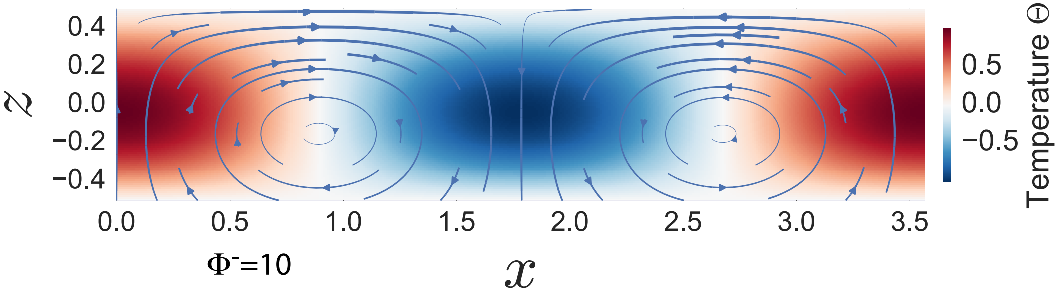

Φ^-=10

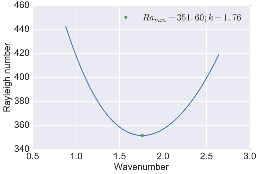

- The flow lines start to cross the bottom boundary.
- The wavelength gets larger and the critical Rayleigh number lower.

Convective modes at onset as function of Φ^- ($\Phi^+ = \infty$)

$\Phi^- = 10^{-2}$:

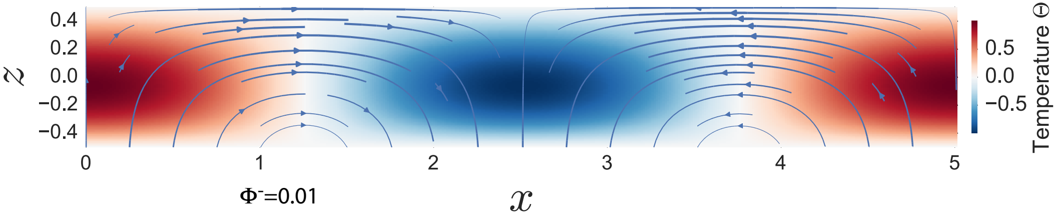

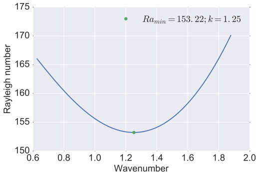

- The wavelength is about twice that for classical boundary conditions and the critical Rayleigh number about a fourth.
- Planform similar to the upper half of a classical convection model.

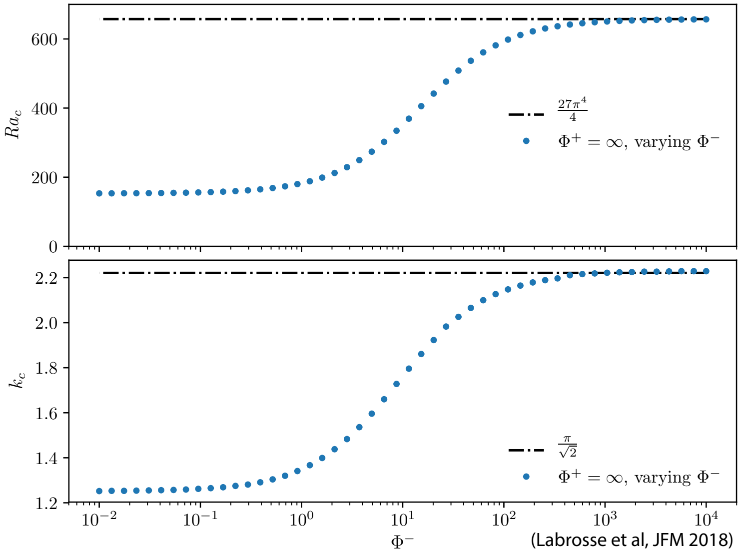

(Labrosse et al, JFM 2018)

Ra_c decreased by a factor ~ 4, k_c decreased by a factor ~ 2

Weakly non-linear results

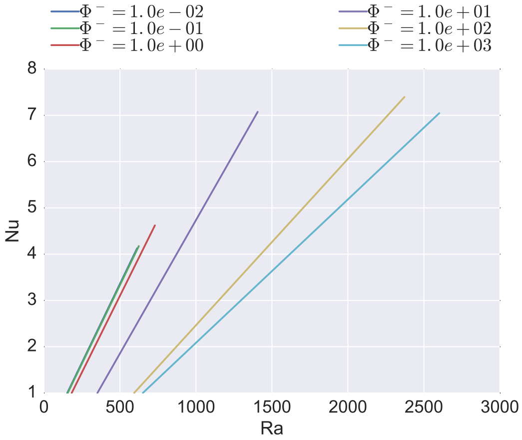

- Decreasing $\Phi^{\pm}$, the dimension-less heat flux (Nusselt number, Nu) increases:
  - because of the decrease of Ra_c.
  - because the slope $\mathrm{d}Nu/\,\mathrm{d}Ra$ increases by a factor ~ 2 when $\Phi^- \to 0$.

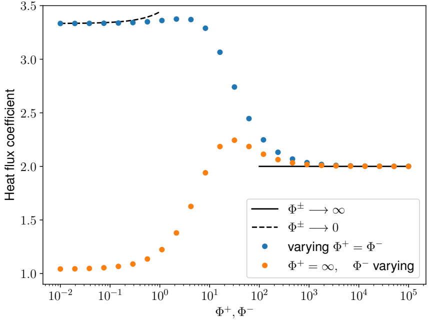

Thermal structure with one boundary with $\Phi = 0.1$

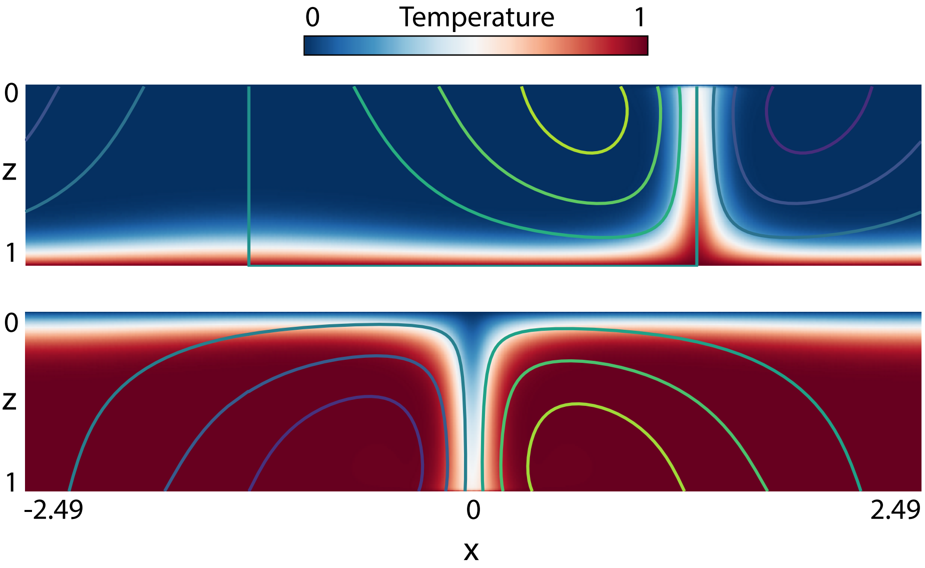

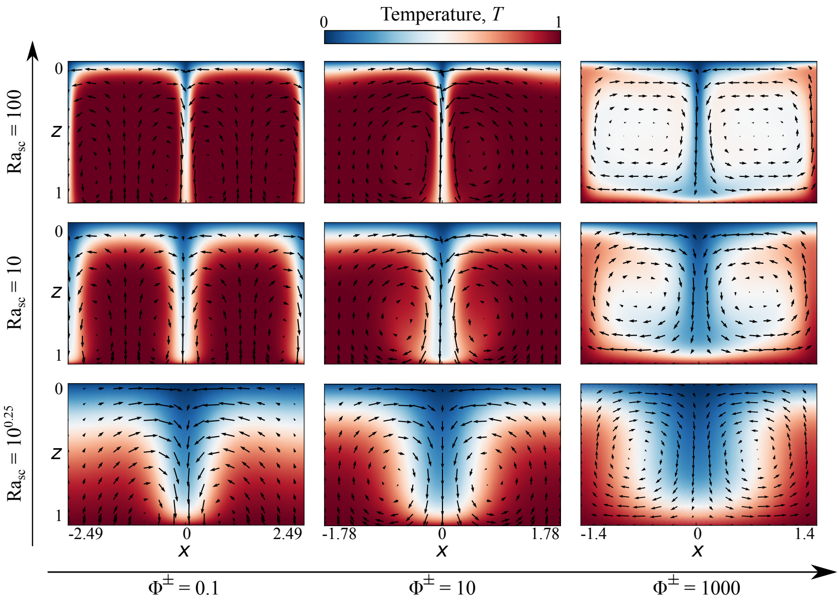

Temperature, T
0
1
$\mathrm{Ra}_{sc} = 100$
$\mathrm{Ra}_{sc} = 10$
$\mathrm{Ra}_{sc} = 10^{0.25}$
z
0
1
-2.49
0
2.49
-1.78
1.78
-1.4
1.4
x
$\Phi^{\pm} = 0.1$
$\Phi^{\pm} = 10$
$\Phi^{\pm} = 1000$

Heat transfer and mean temperature - close to onset

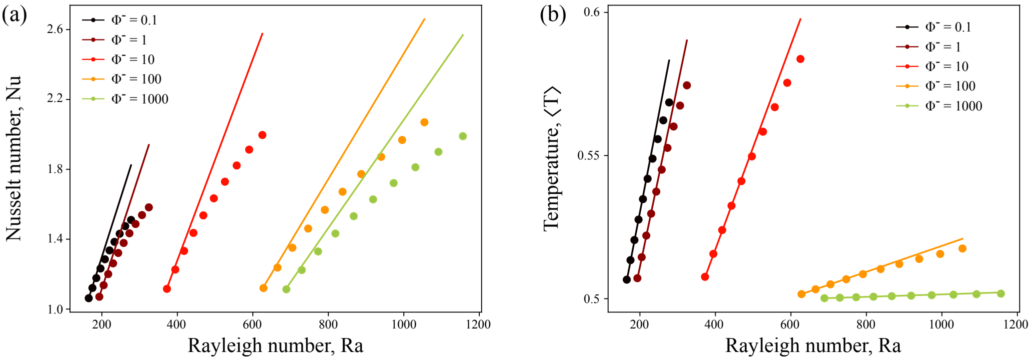

- Good match of the fully non–linear results (DNS) and the weakly non–linear ones for small Ra/Ra_c.
- Deviation at high Ra, more rapidly for heat flow (Nusselt number) than average temperature.

Heat transfer and mean temperature - high Rayleigh number

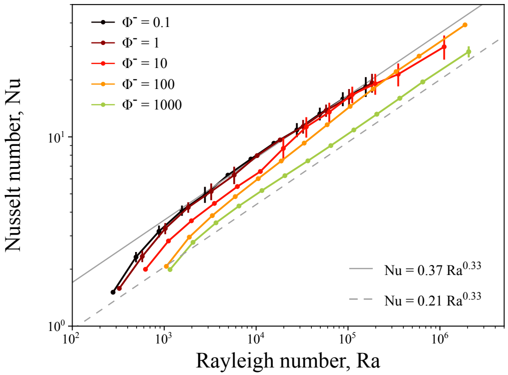

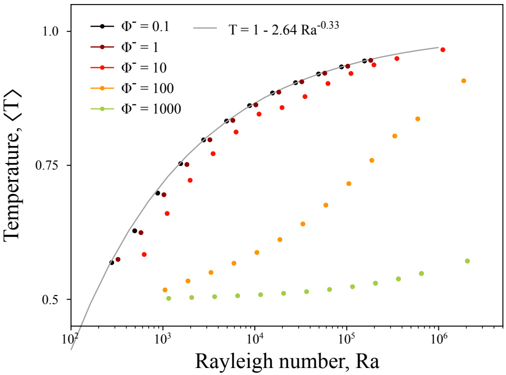

- At high *Ra*, $Nu \sim C Ra^{1/3}$.
- Coefficient C larger for small $\Phi \Rightarrow$ heat flow about twice larger for a given *Ra*.
- Consistent with a dynamics controlled by the only active boundary layer.

Outline

Spherical shell geometry

Extension to spherical shell geometry performed by Adrien Morison during his PhD thesis (defended Nov. 15th).

- An additional parameter: the aspect ratio $\gamma = R^- / R^+$
- Linear stability analysis.
- Application to the onset of convection during magma ocean crystallisation (Morison et al., 2019).
- Direct numerical simulations.

Linear stability analysis

- Equations are linearly developed around the conductive steady-state solution.
- Viscosity is only z-dependent

$$\Rightarrow \mathbf{u} = \boldsymbol{\nabla} \times \boldsymbol{\nabla} \times (\mathcal{P}\mathbf{r})$$

- Separation of variables:

$$\mathcal{P} = \sum_{l=1}^{\infty} \sum_{m=-l}^{l} P_l^m(r) Y_l^m(\theta, \varphi) e^{\sigma_l t}$$

- Discretization along radial direction with Chebyshev polynomials
  - Harmonic degree l plays the role of the wavenumber.
  - How do Ra_c and l_c depend on Φ^+ and Φ^-?

- Equations are linearly developed around the conductive steady-state solution.
- Viscosity is only z-dependent

$$\Rightarrow \mathbf{u} = \boldsymbol{\nabla} \times \boldsymbol{\nabla} \times (\mathcal{P}\mathbf{r})$$

- Separation of variables:

$$\mathcal{P} = \sum_{l=1}^{\infty} \sum_{m=-l}^{l} P_l^m(r)\, Y_l^m(\theta, \varphi) e^{\sigma_l t}$$

- Discretization along radial direction with Chebyshev polynomials
  - Harmonic degree l plays the role of the wavenumber.
  - How do Ra_c and l_c depend on Φ^+ and Φ^-?

- Equations are linearly developed around the conductive steady-state solution.
- Viscosity is only z-dependent

$$\Rightarrow \mathbf{u} = \boldsymbol{\nabla} \times \boldsymbol{\nabla} \times (\mathcal{P}\mathbf{r})$$

- Separation of variables:

$$\mathcal{P} = \sum_{l=1}^{\infty} \sum_{m=-l}^{l} P_l^m(r)\, Y_l^m(\theta, \varphi) e^{\sigma_l t}$$

- Discretization along radial direction with Chebyshev polynomials
  - Harmonic degree l plays the role of the wavenumber.
  - How do Ra_c and l_c depend on Φ^+ and Φ^-?

Purely thermal and no net freezing case

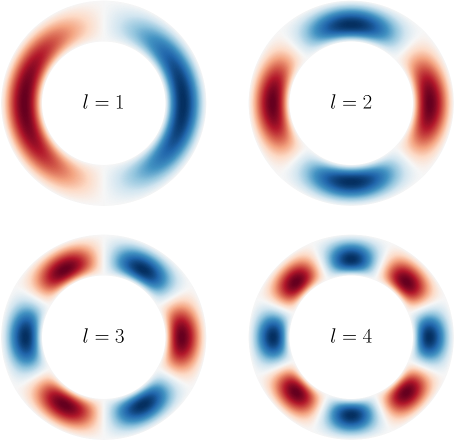

...

Perturbation of conductive state

- Choose a degree l (number of hot patches)
- Look for the *neutral Rayleigh number* above which the perturbation grows
- Scan through values of l to find the one with the minimal neutral Rayleigh number $\rightarrow Ra_c$ and associated l_c

The conductive state is unstable if:

$$Ra > Ra_c$$

Effects of the aspect ratio ($\gamma = \frac{R^-}{R^+}$) and the presence of magma oceans ($\Phi^\pm$) on Ra_c and l_c?

Purely thermal and no net freezing case

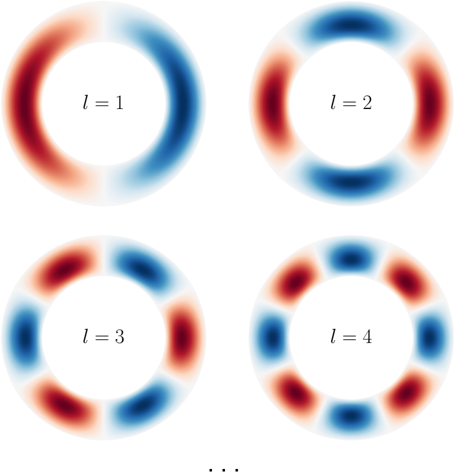

Perturbation of conductive state

- Choose a degree l (number of hot patches)
- Look for the *neutral Rayleigh number* above which the perturbation grows
- Scan through values of l to find the one with the minimal neutral Rayleigh number $\rightarrow Ra_c$ and associated l_c

The conductive state is unstable if:

$$Ra > Ra_c$$

Effects of the aspect ratio ($\gamma = \frac{R^-}{R^+}$) and the presence of magma oceans ($\Phi^{\pm}$) on Ra_c and l_c?

Purely thermal and no net freezing case

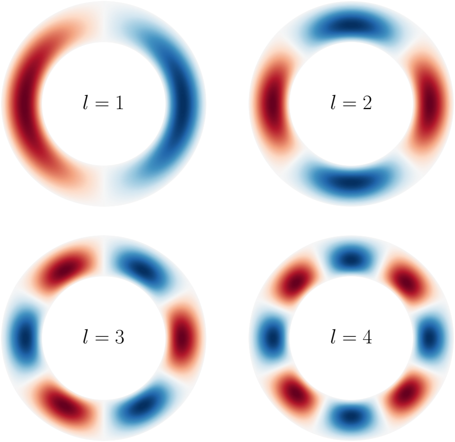

...

Perturbation of conductive state

- Choose a degree l (number of hot patches)
- Look for the *neutral Rayleigh number* above which the perturbation grows
- Scan through values of l to find the one with the minimal neutral Rayleigh number $\rightarrow Ra_c$ and associated l_c

The conductive state is unstable if:

$$Ra > Ra_c$$

Effects of the aspect ratio ($\gamma = \frac{R^-}{R^+}$) and the presence of magma oceans ($\Phi^{\pm}$) on Ra_c and l_c?

Purely thermal and no net freezing case

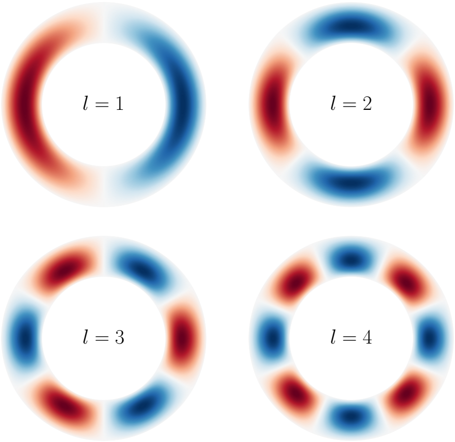

. . .

Perturbation of conductive state

- Choose a degree l (number of hot patches)
- Look for the *neutral Rayleigh number* above which the perturbation grows
- Scan through values of l to find the one with the minimal neutral Rayleigh number $\rightarrow$ Ra_c and associated l_c

The conductive state is unstable if:

$$Ra > Ra_c$$

Effects of the aspect ratio ($\gamma = \frac{R^-}{R^+}$) and the presence of magma oceans ($\Phi^{\pm}$) on Ra_c and l_c?

Purely thermal and no net freezing case

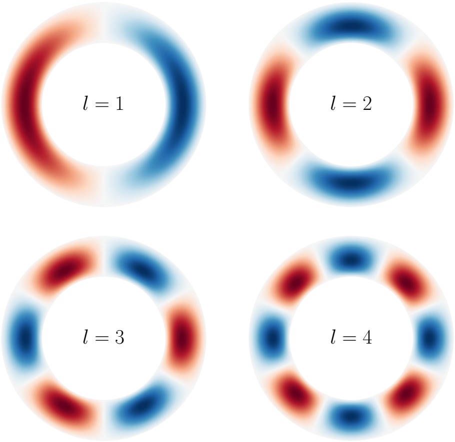

. . .

Perturbation of conductive state

- Choose a degree l (number of hot patches)
- Look for the *neutral Rayleigh number* above which the perturbation grows
- Scan through values of l to find the one with the minimal neutral Rayleigh number $\rightarrow Ra_c$ and associated l_c

The conductive state is unstable if:

$$Ra > Ra_c$$

Effects of the aspect ratio ($\gamma = \frac{R^-}{R^+}$) and the presence of magma oceans ($\Phi^{\pm}$) on Ra_c and l_c?

Linear Stability – Results

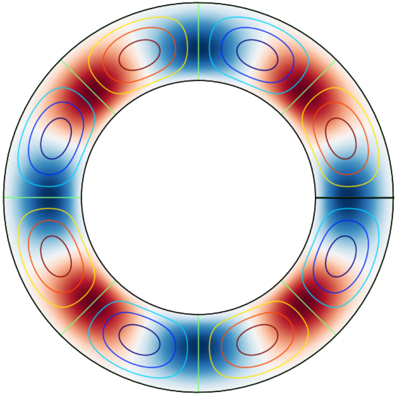

$$\Phi^+ = 10^4$$
$$\Phi^- = 10^4$$

- $Ra_c = 687$ and $l_c = 4$
- Roughly square rolls
- Similar to classic non-permeable case

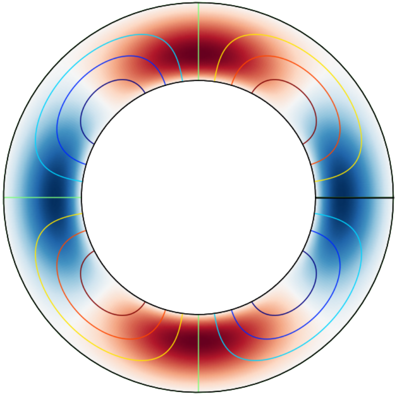

$$\Phi^+ = 10^4$$
$$\Phi^- = 10^{-2}$$

- $Ra_c = 188$ and $l_c = 2$
- Flow-through at the bottom
  - Half cells
  - Twice as wide
- Return current in the liquid ocean

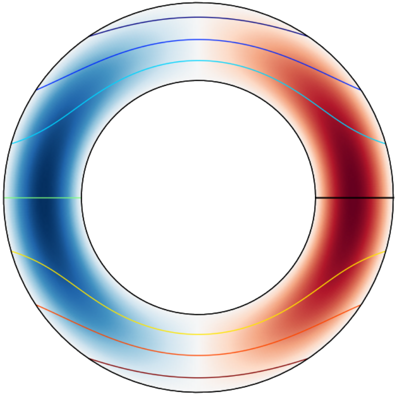

$$\Phi^{+} = 10^{-2}$$
$$\Phi^{-} = 10^{4}$$

- $Ra_c = 96$ and $l_c = 1$
- Quasi-translation mode
- Very little deformation in the solid

Linear Stability – Results

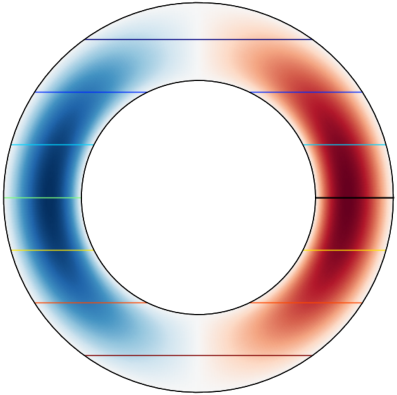

$$\Phi^+ = 10^{-2}$$
$$\Phi^- = 10^{-2}$$

- $Ra_c = 0.11$ and $l_c = 1$
- Translation mode without deformation
- Only limited by phase change

Effect of γ – Classical case

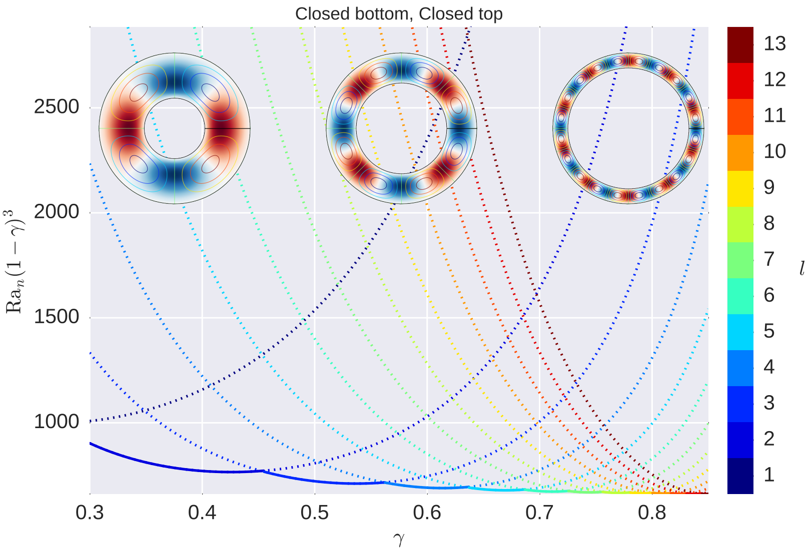

Effect of γ – Open at the bottom

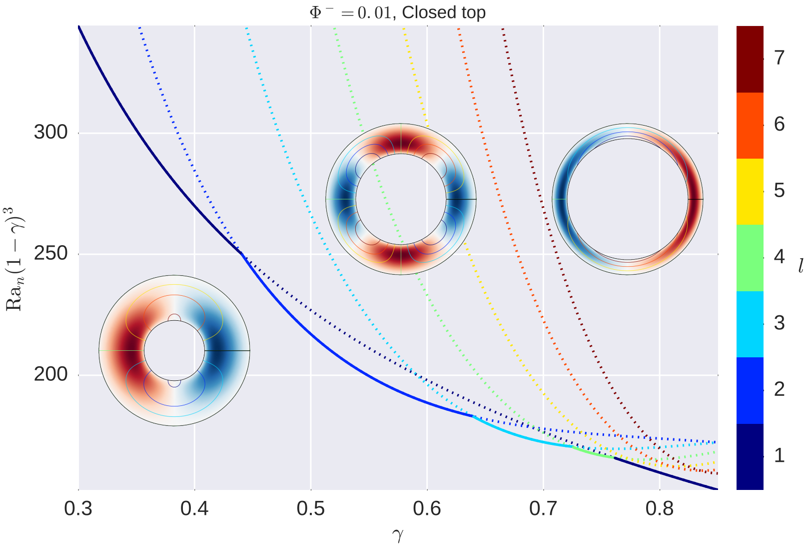

Competition between modes

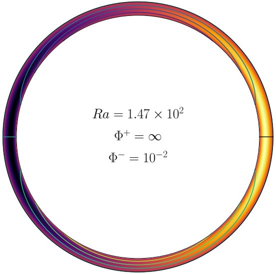

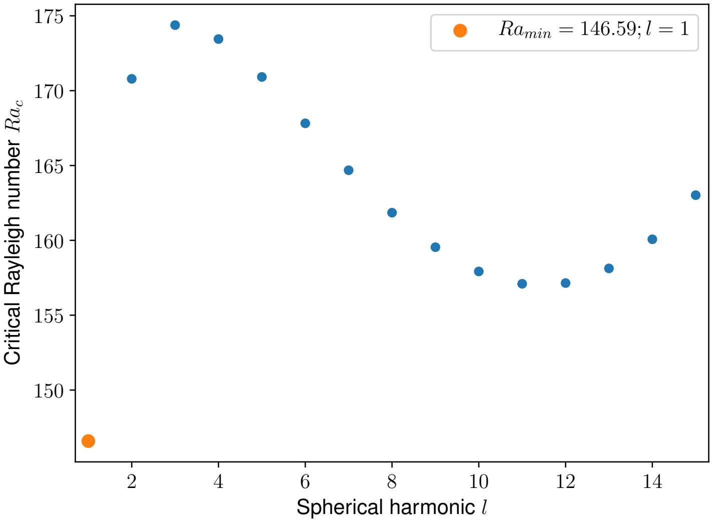

Effect of γ – Open at the top

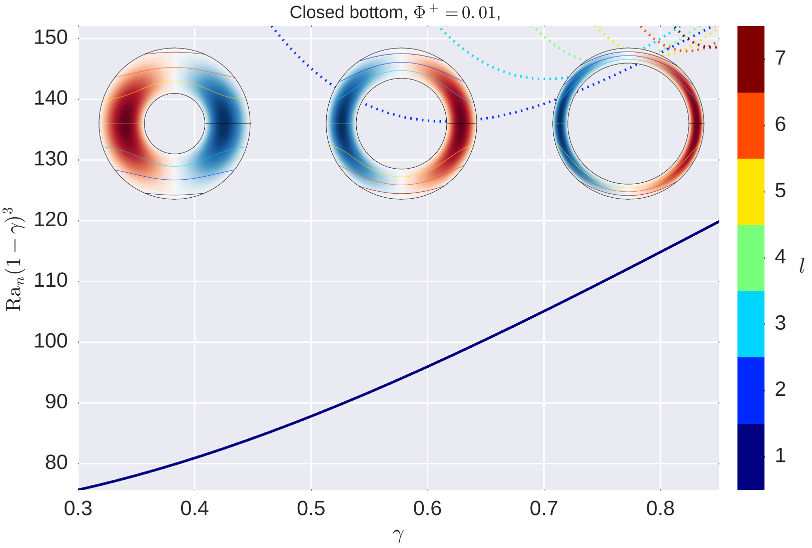

Effect of γ – Open at both boundaries

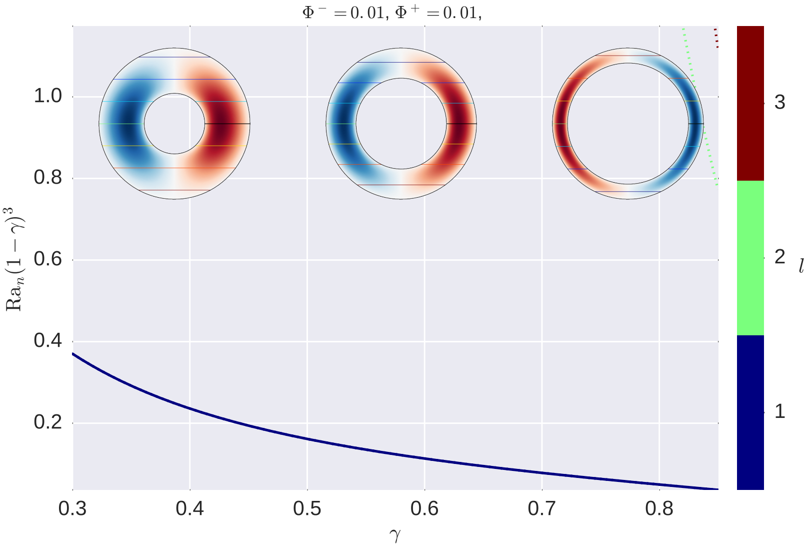

Exploration of parameter space $(\gamma, \Phi^{\pm})$

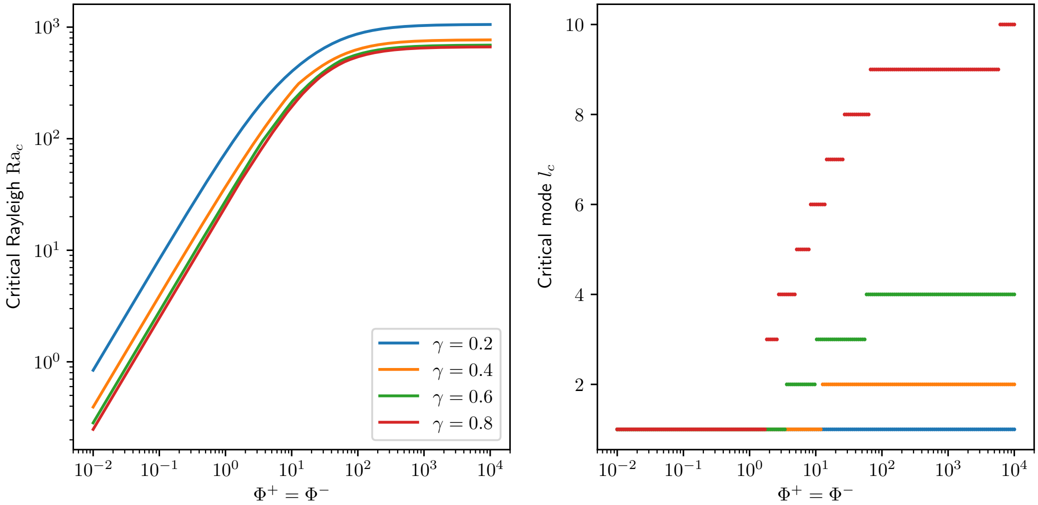

- Using StagYY (Tackley, 2008) in the spherical annulus geometry (Hernlund and Tackley, 2008).

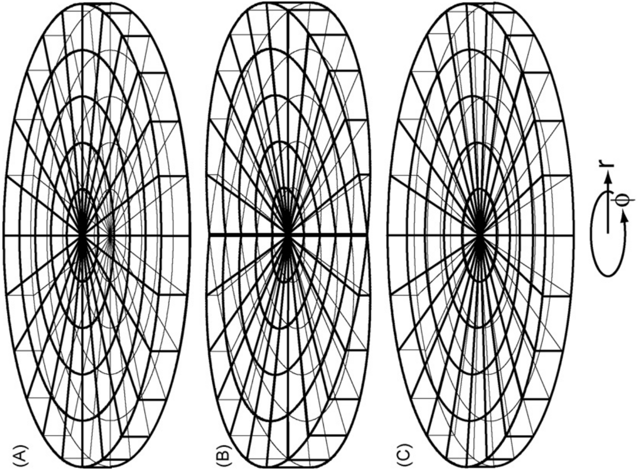

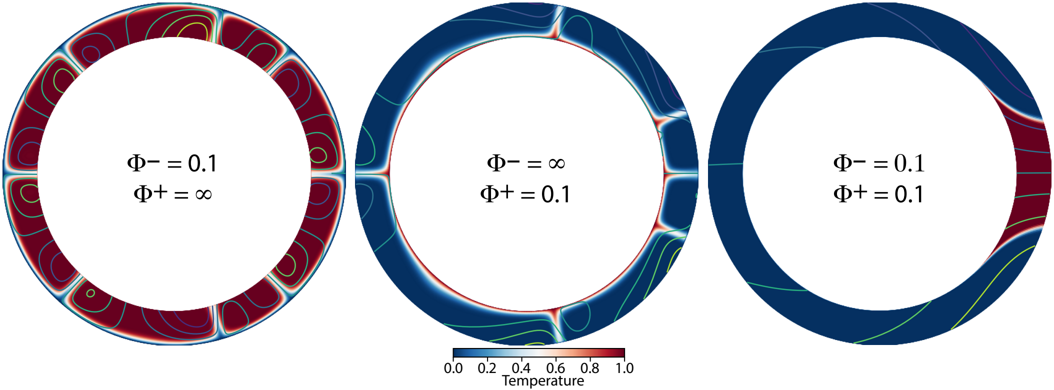

- $Ra = 100$
- Difference with the cartesian geometry: the translation mode is degree 1, not 0.
- Translation shows some deformation.

$Ra = \sqrt{10}Ra_c$; $\Phi^- = \infty$; $\Phi^+ = 10^{-2}$; $\gamma = 0.6$

- Starts as $l = l_c = 1$
- Unstable to perturbations with $l = 2, 3$

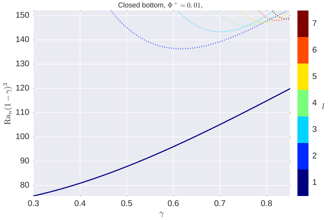

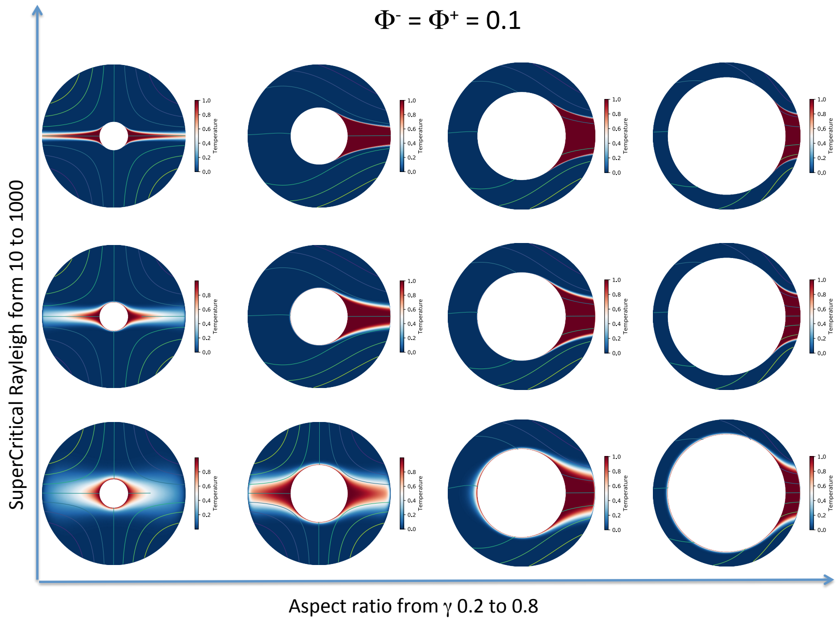

Φ⁻ = Φ⁺ = 0.1
SuperCritical Rayleigh form 10 to 1000
Aspect ratio from γ 0.2 to 0.8
Temperature

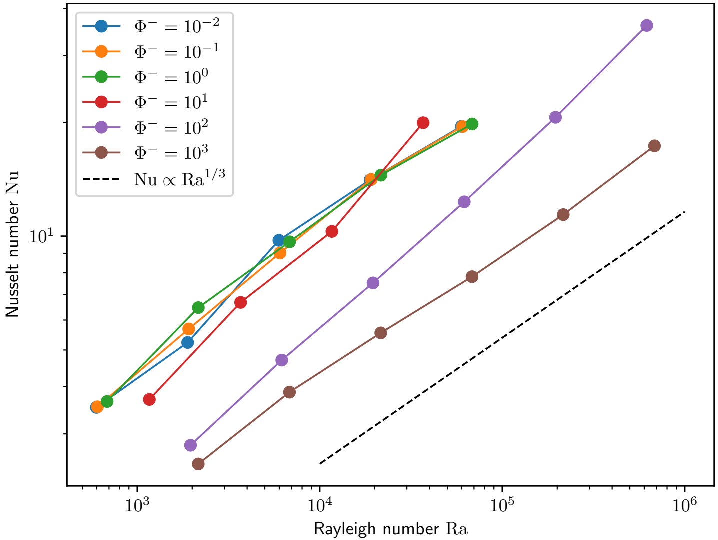

Similarly to cartesian geometry:

- Convection controlled by the dynamic of the only active boundary layer

$\Rightarrow$ $Nu \sim Ra^{1/3}$

Heat flux with two oceans

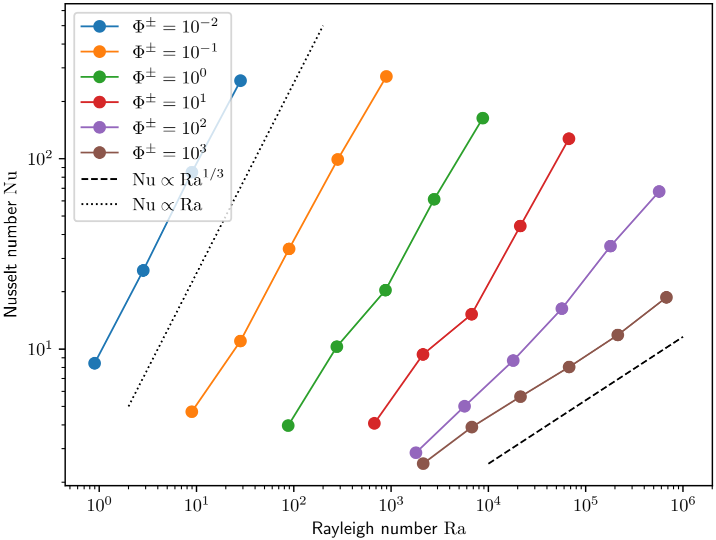

Similarly to cartesian geometry:

- Convection at low Φ not impeded by viscous deformation

$\Rightarrow$ *Nu* $\sim$ *Ra*.

Magma ocean

- Lunar observations: the magma ocean concept.
- Generally thought to crystallise very fast.
- First cristallisation depends on the relative shapes of the liquidus and the isentrope.

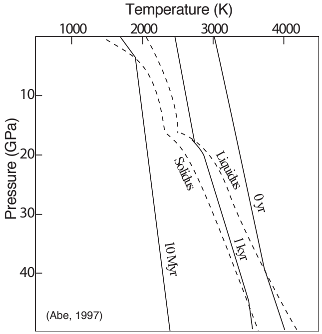

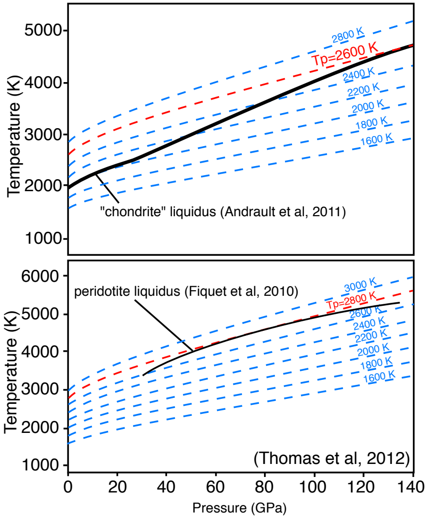

Upward fractional crystallisation of a magma ocean

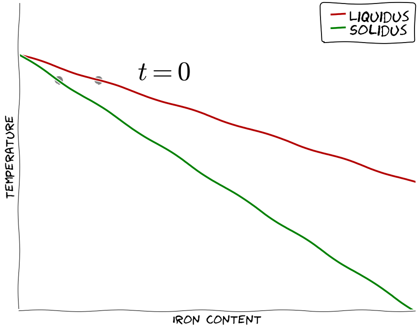

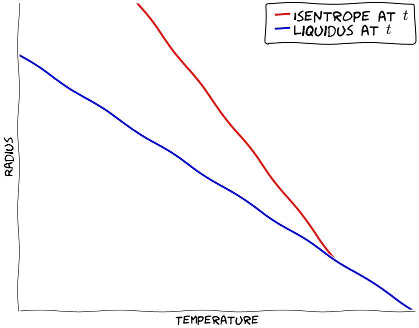

- Solid depleted in Fe compared to the liquid $\Rightarrow$ the liquid gets enriched with time and so does the solid as a result.
- The liquidus temperature decreases with time.
- The solid formed is both thermally and compositionally unstably stratified $\Rightarrow$ prone to overturn (Hess, Parmentier, Elkins-Tanton et al.)

Upward fractional crystallisation of a magma ocean

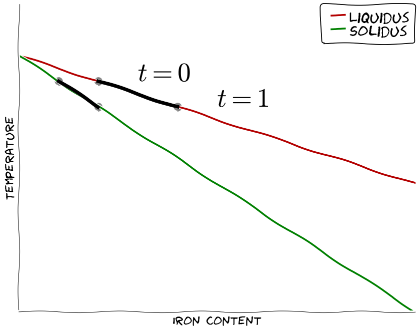

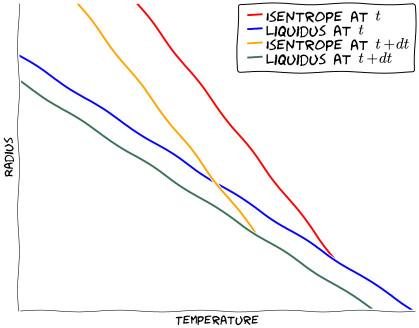

- Solid depleted in Fe compared to the liquid $\Rightarrow$ the liquid gets enriched with time and so does the solid as a result.
- The liquidus temperature decreases with time.
- The solid formed is both thermally and compositionally unstably stratified $\Rightarrow$ prone to overturn (Hess, Parmentier, Elkins-Tanton et al.)

Upward fractional crystallisation of a magma ocean

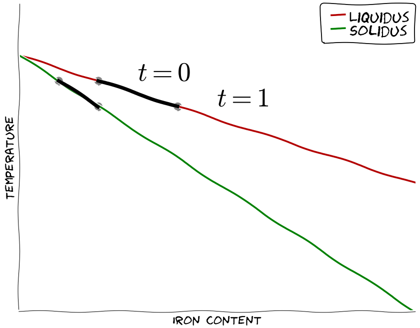

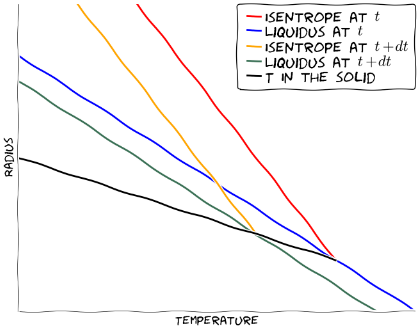

- Solid depleted in Fe compared to the liquid $\Rightarrow$ the liquid gets enriched with time and so does the solid as a result.
- The liquidus temperature decreases with time.
- The solid formed is both thermally and compositionally unstably stratified $\Rightarrow$ prone to overturn (Hess, Parmentier, Elkins-Tanton et al.)

Effect of the solid/liquid partition coefficient

A simple theoretical calculation for a constant partition coefficient.

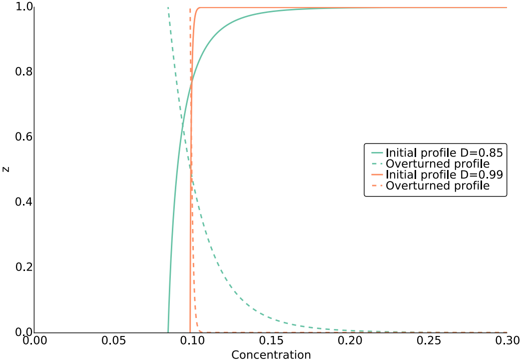

Thermal and compositional structure of MO and its crystallisation more complicated.

Overturn of the solid mantle after its upward crystallisation

Concentration:

Temperature:

Composition and temperature profiles during overturn

Concentration:

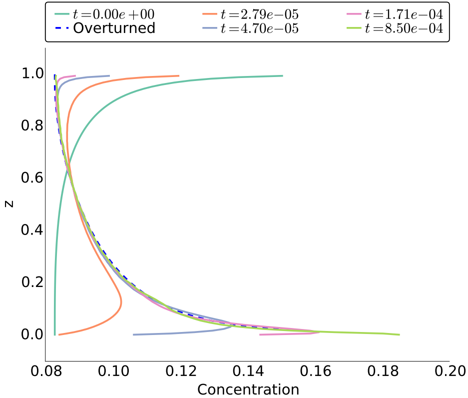

Temperature:

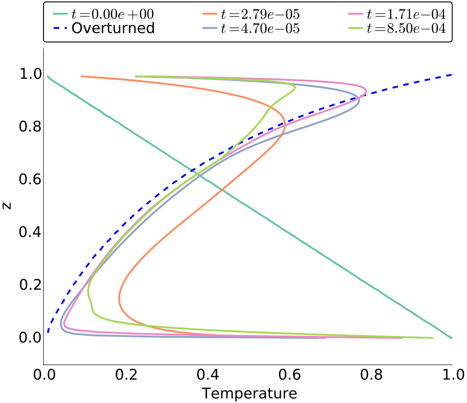

- Well explained by simple rearengement according to density (justifying the hypoteses in Elkins-Tanton et al's studies).
- Temperature: extra effect of diffusion and boundary conditions.

Composition and temperature profiles after overturn

Concentration:

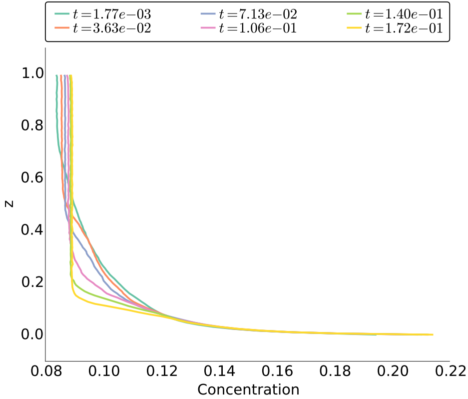

Temperature:

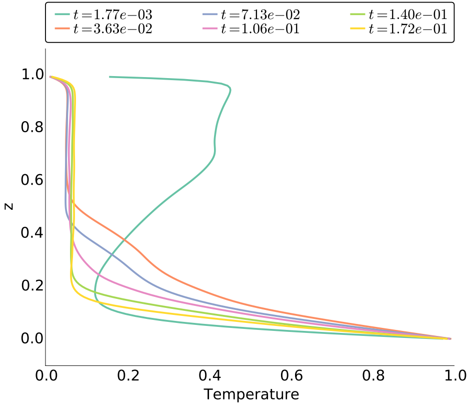

- After overturn, temperature and composition profiles show slow entrainment of the lower layer by convection in the upper one.
- Does the overturn wait for complete crystallisation to proceed? Compute the growth–rate of the instability.

Model of crystallization
Morison et al. (2019)

- Well mixed SMO
- $\bar{C}(R^+) = DC_l$
- $\bar{T} = T_{\text{sol}} = f(P, C)$
- $\varepsilon\sigma(T_s^4 - T_\infty^4) \propto Ra_O^{2/7}$ (King *et al.*, 2012)

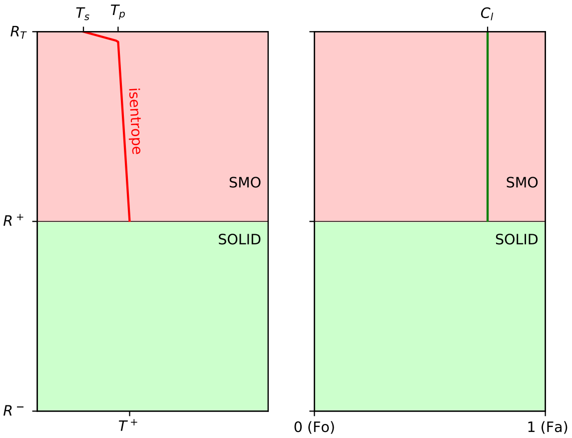

$\rightarrow R^+(t)$, $\bar{T}(r)$ and $\bar{C}(r)$ in solid

Solid is gravitationally unstable $\Rightarrow$ **When does convection start?**

Control parameters: emissivity ε and partition coefficient D

Model of crystallization
Morison et al. (2019)

- Well mixed SMO
- $\bar{C}(R^+) = DC_l$
- $\bar{T} = T_{\text{sol}} = f(P, C)$
- $\varepsilon\sigma(T_s^4 - T_\infty^4) \propto Ra_O^{2/7}$ (King *et al.*, 2012)

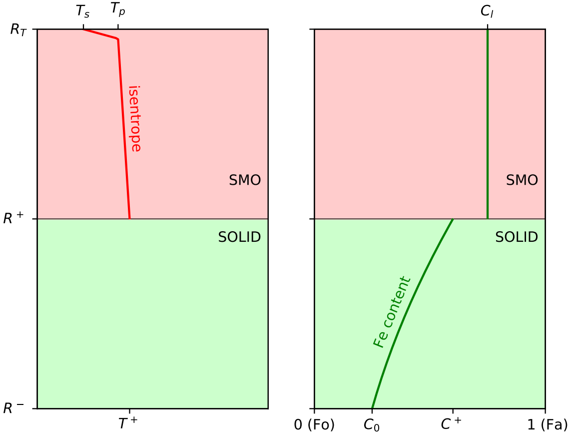

$\rightarrow R^+(t)$, $\bar{T}(r)$ and $\bar{C}(r)$ in solid

Solid is gravitationally unstable $\Rightarrow$ **When does convection start?**

Control parameters: emissivity ε and partition coefficient D

Model of crystallization
Morison et al. (2019)

- Well mixed SMO
- $\bar{C}(R^+) = DC_l$
- $\bar{T} = T_{\text{sol}} = f(P, C)$
- $\varepsilon\sigma(T_s^4 - T_\infty^4) \propto Ra_O^{2/7}$ (King *et al.*, 2012)

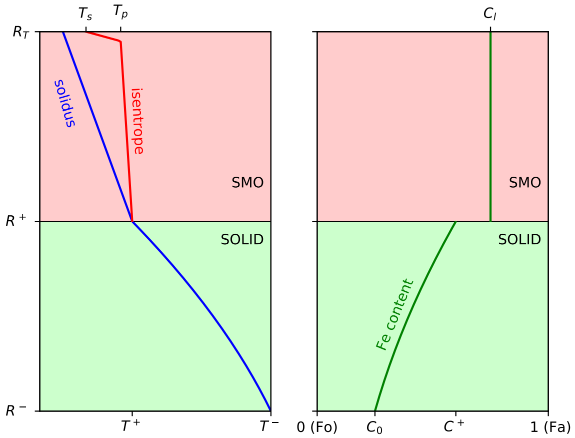

$\rightarrow R^+(t)$, $\bar{T}(r)$ and $\bar{C}(r)$ in solid

Solid is gravitationally unstable $\Rightarrow$ **When does convection start?**

Control parameters: emissivity ε and partition coefficient D

Model of crystallization
Morison et al. (2019)

- Well mixed SMO
- $\bar{C}(R^+) = DC_l$
- $\bar{T} = T_{\text{sol}} = f(P, C)$
- $\varepsilon\sigma(T_s^4 - T_\infty^4) \propto Ra_O^{2/7}$ (King *et al.*, 2012)

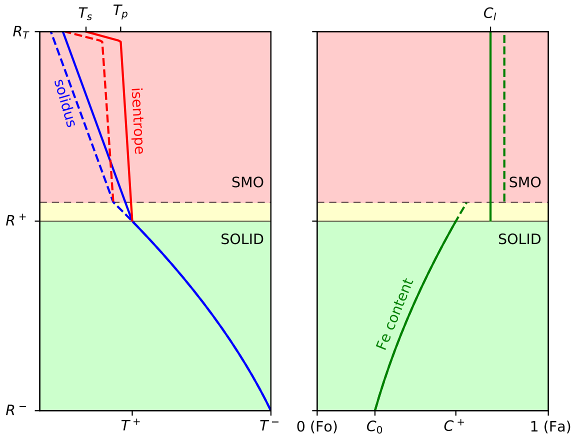

$\rightarrow R^+(t)$, $\bar{T}(r)$ and $\bar{C}(r)$ in solid

Solid is gravitationally unstable $\Rightarrow$ **When does convection start?**

Control parameters: emissivity ε and partition coefficient D

Model of crystallization
Morison et al. (2019)

- Well mixed SMO
- $\bar{C}(R^+) = DC_l$
- $\bar{T} = T_{\text{sol}} = f(P, C)$
- $\varepsilon\sigma(T_s^4 - T_\infty^4) \propto Ra_O^{2/7}$ (King *et al.*, 2012)

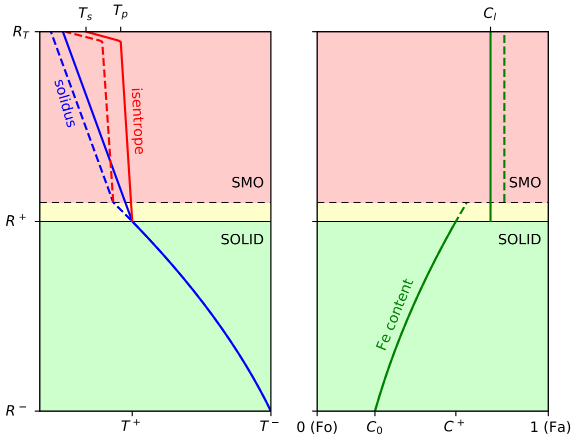

$\rightarrow R^+(t)$, $\bar{T}(r)$ and $\bar{C}(r)$ in solid

Solid is gravitationally unstable $\Rightarrow$ **When does convection start?**

Control parameters: emissivity ε and partition coefficient D

Model of crystallization
Morison et al. (2019)

- Well mixed SMO
- $\bar{C}(R^+) = DC_l$
- $\bar{T} = T_{\text{sol}} = f(P, C)$
- $\varepsilon\sigma(T_s^4 - T_\infty^4) \propto Ra_O^{2/7}$ (King *et al.*, 2012)

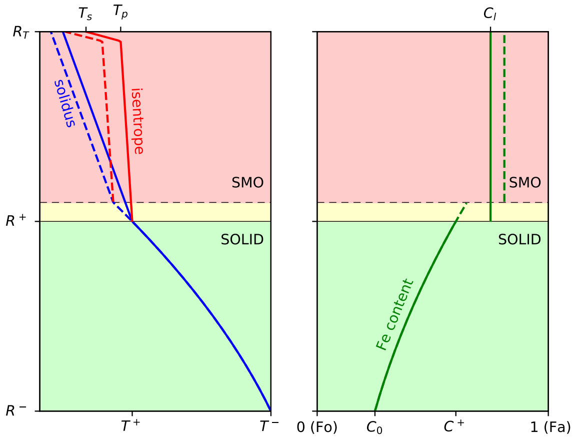

$\rightarrow R^+(t)$, $\bar{T}(r)$ and $\bar{C}(r)$ in solid

Solid is gravitationally unstable $\Rightarrow$ **When does convection start?**

Control parameters: emissivity ε and partition coefficient D

Model of crystallization
Morison et al. (2019)

- Well mixed SMO
- $\bar{C}(R^+) = DC_l$
- $\bar{T} = T_{\text{sol}} = f(P, C)$
- $\varepsilon\sigma(T_s^4 - T_\infty^4) \propto Ra_O^{2/7}$ (King *et al.*, 2012)

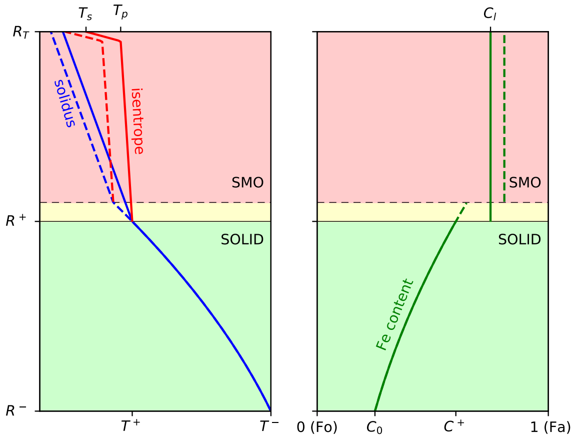

$\rightarrow R^+(t)$, $\bar{T}(r)$ and $\bar{C}(r)$ in solid

Solid is gravitationally unstable $\Rightarrow$ **When does convection start?**

Control parameters: emissivity ε and partition coefficient D

Model of crystallization
Morison et al. (2019)

- Well mixed SMO
- $\bar{C}(R^+) = DC_l$
- $\bar{T} = T_{\text{sol}} = f(P, C)$
- $\varepsilon\sigma(T_s^4 - T_\infty^4) \propto Ra_O^{2/7}$ (King *et al.*, 2012)

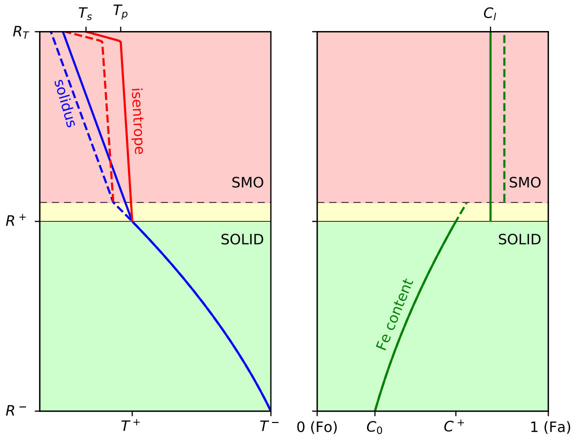

$\rightarrow R^+(t)$, $\bar{T}(r)$ and $\bar{C}(r)$ in solid

Solid is gravitationally unstable $\Rightarrow$ **When does convection start?**

Control parameters: emissivity ε and partition coefficient D

Net crystallization: $\dot{R}^+$, $\dot{R}^-$, $\dot{T}^+$, $\dot{T}^-$ (model of magma ocean cooling)

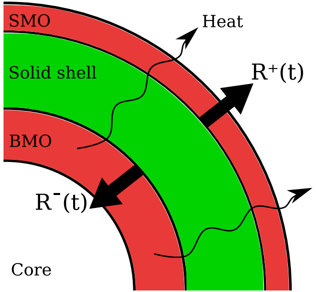

The computational dimensionless domain has fixed boundaries:

$$\tilde{r} = 1 + \frac{r - R^-(t)}{L(t)} \Rightarrow 1 \leqslant \tilde{r} \leqslant 2$$

$$\tilde{T} = \frac{T - T^+(t)}{\Delta T(t)} \Rightarrow 0 \leqslant \tilde{T} \leqslant 1$$

Conservation equations written in that frame

Scales for time $t = \tilde{t}\frac{L_M^2}{\kappa}$, distance $x = \tilde{x}L(t)$, velocity $u = \tilde{u}\frac{\kappa}{L(t)}$

Net crystallization: $\dot{R}^+$, $\dot{R}^-$, $\dot{T}^+$, $\dot{T}^-$ (model of magma ocean cooling)

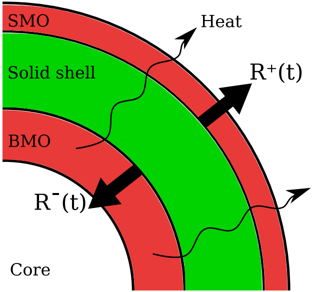

The computational dimensionless domain has fixed boundaries:

$$\tilde{r} = 1 + \frac{r - R^-(t)}{L(t)} \Rightarrow 1 \leqslant \tilde{r} \leqslant 2$$

$$\tilde{T} = \frac{T - T^+(t)}{\Delta T(t)} \Rightarrow 0 \leqslant \tilde{T} \leqslant 1$$

Conservation equations written in that frame

Scales for time $t = \tilde{t}\frac{L_M^2}{\kappa}$, distance $x = \tilde{x}L(t)$, velocity $u = \tilde{u}\frac{\kappa}{L(t)}$

Net crystallization: $\dot{R}^+$, $\dot{R}^-$, $\dot{T}^+$, $\dot{T}^-$ (model of magma ocean cooling)

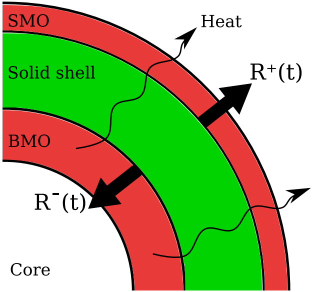

The computational dimensionless domain has fixed boundaries:

$$\tilde{r} = 1 + \frac{r - R^-(t)}{L(t)} \Rightarrow 1 \leqslant \tilde{r} \leqslant 2$$

$$\tilde{T} = \frac{T - T^+(t)}{\Delta T(t)} \Rightarrow 0 \leqslant \tilde{T} \leqslant 1$$

Conservation equations written in that frame

Scales for time $t = \tilde{t}\frac{L_M^2}{\kappa}$, distance $x = \tilde{x}L(t)$, velocity $u = \tilde{u}\frac{\kappa}{L(t)}$

Destabilization timescale – Linear stability analysis

Cooling model $\rightarrow R^+(t),\ \dot{R}^+(t),\ \bar{T}(r),\ \bar{C}(r),\ \mathit{Ra}(t),\ \mathit{Ra}(t)$

- At any given time, look for most unstable l, here $l = 1$

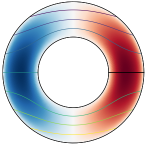

- Destabilization time scale $1/\sigma$
- Compared to time needed to crystallize remaining MO

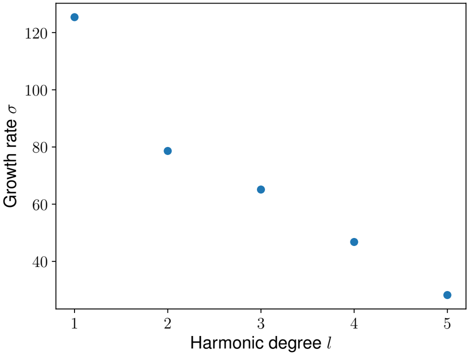

Cooling model $\rightarrow R^+(t),\ \dot{R}^+(t),\ \bar{T}(r),\ \bar{C}(r),\ \mathit{Ra}(t),\ \mathit{Ra}(t)$

- At any given time, look for most unstable l, here $l = 1$

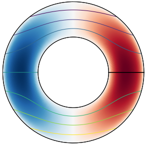

- Destabilization time scale $1/\sigma$
- Compared to time needed to crystallize remaining MO

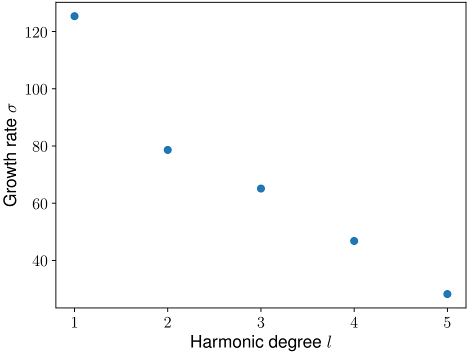

Cooling model $\rightarrow R^{+}(t),\ \dot{R}^{+}(t),\ \bar{T}(r),\ \bar{C}(r),\ \mathit{Ra}(t),\ \mathit{Ra}(t)$

- At any given time, look for most unstable l, here $l = 1$

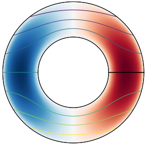

- Destabilization time scale $1/\sigma$
- Compared to time needed to crystallize remaining MO

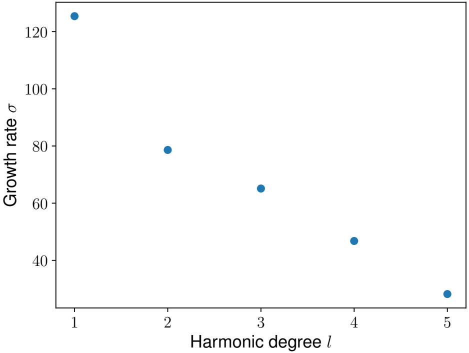

Destabilization timescale – Linear stability analysis

Cooling model $\rightarrow R^+(t)$, $\dot{R}^+(t)$, $\bar{T}(r)$, $\bar{C}(r)$, $Ra(t)$, $Ra(t)$

- At any given time, look for most unstable l, here $l = 1$

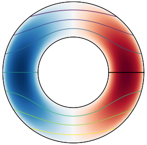

- Destabilization time scale $1/\sigma$
- Compared to time needed to crystallize remaining MO

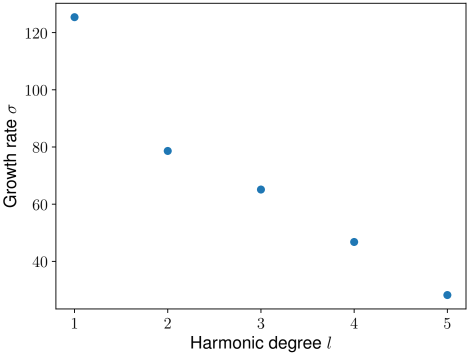

Destabilization times for terrestrial bodies
Morison et al. (2019)

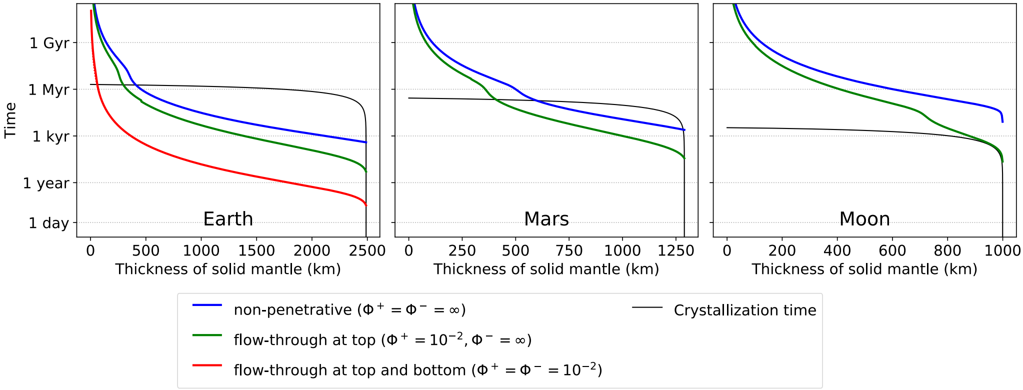

- Convection sets in the solid before the entire crystallization
  - For the Moon, plagioclase crust delays the end of crystallization
- Phase change boundary leads to earlier onset and degree $l = 1$

Important role for the long term evolution of the system!

Destabilization times for terrestrial bodies
Morison et al. (2019)

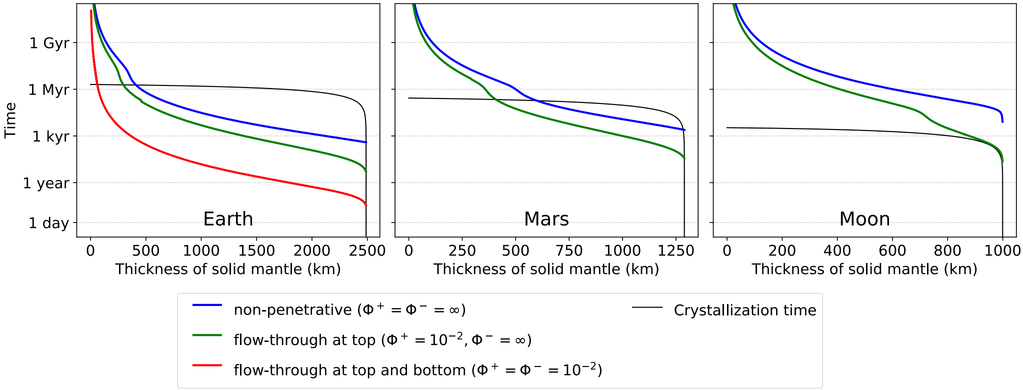

- Convection sets in the solid before the entire crystallization
  - For the Moon, plagioclase crust delays the end of crystallization
- Phase change boundary leads to earlier onset and degree $l = 1$

Important role for the long term evolution of the system!

Destabilization times for terrestrial bodies
Morison et al. (2019)

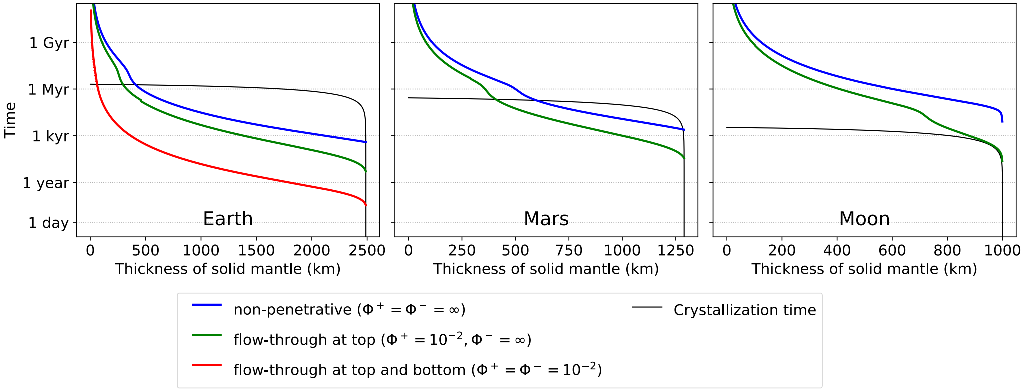

- Convection sets in the solid before the entire crystallization
  - For the Moon, plagioclase crust delays the end of crystallization
- Phase change boundary leads to earlier onset and degree $l = 1$

Important role for the long term evolution of the system!

Destabilization times for terrestrial bodies
Morison et al. (2019)

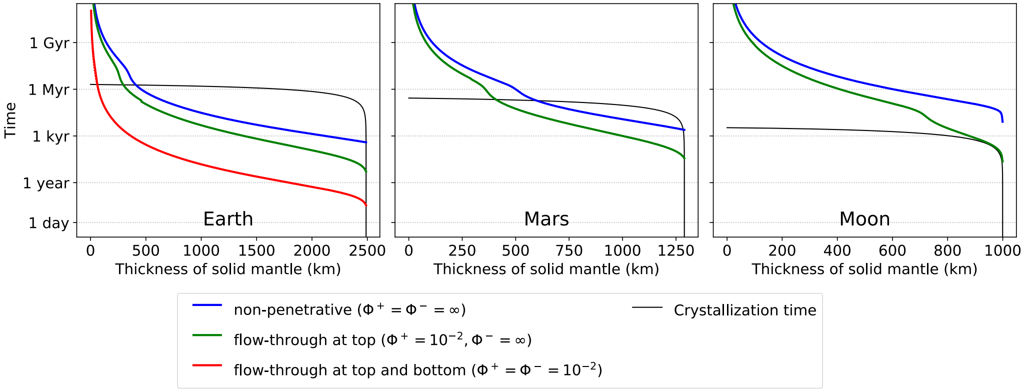

- Convection sets in the solid before the entire crystallization
  - For the Moon, plagioclase crust delays the end of crystallization
- Phase change boundary leads to earlier onset and degree $l = 1$

Important role for the long term evolution of the system!

Destabilisation time vs. crystallisation time

Morison et al. (2019)

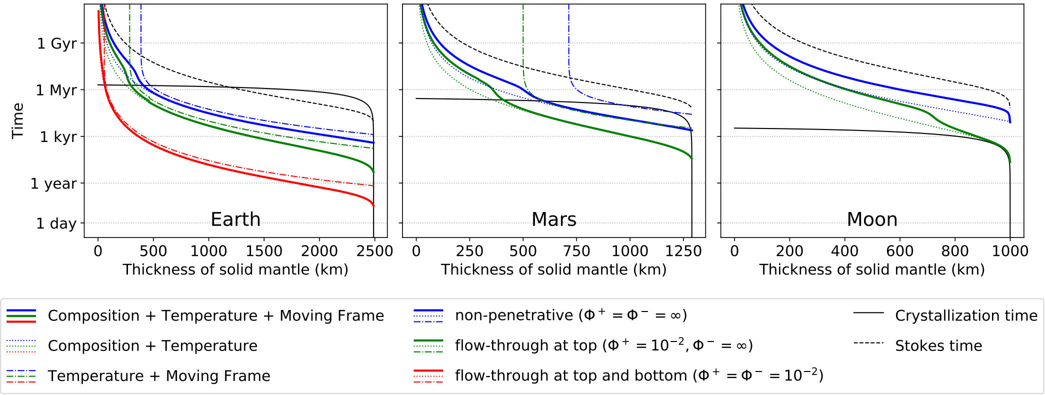

- Destabilisation before complete crystallisation
- Destabilisation eased by the possibility of phase change at either or, even more, both boundaries.
- $\Rightarrow$ magma ocean crystallisation has to be included into mantle convection!

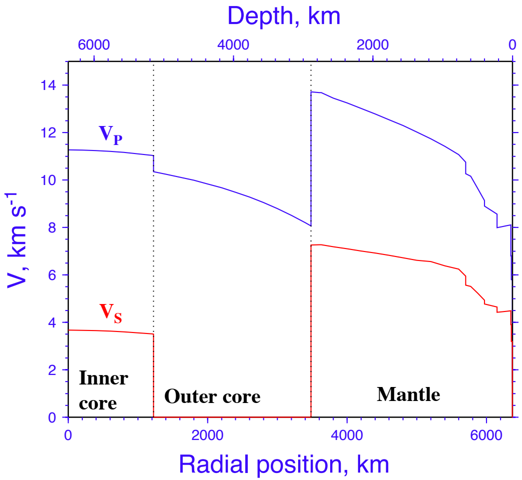

(PREM, Dziewonski & Anderson, 1981)

- Discovered by Inge Lehmann (1936)
- A solid iron ball (mainly) at the center of a liquid iron shell.

⇒ The inner core boundary (ICB) is a phase equilibrium surface.

- Development of inner core seismology has led to the discovery of more and more complex structures.

Structure of the inner core

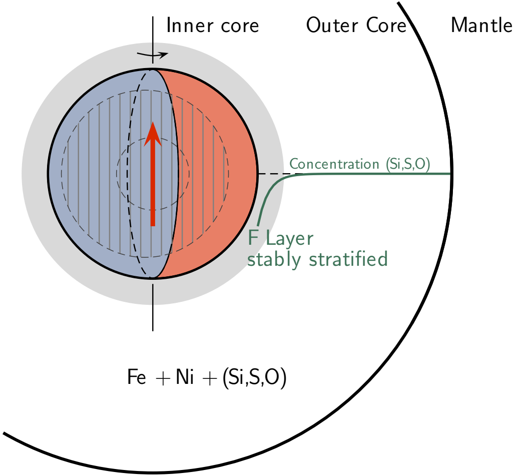

(fig. courtesy of R. Deguen)

- Seismic anisotropy (Morelli et al., 1986; Poupinet et al., 1983; Woodhouse et al., 1986).
- East–west dichotomy, possibly with sharp edges.
- A different innermost inner core.
- These observations call for one or more explanations.

Structure of the inner core

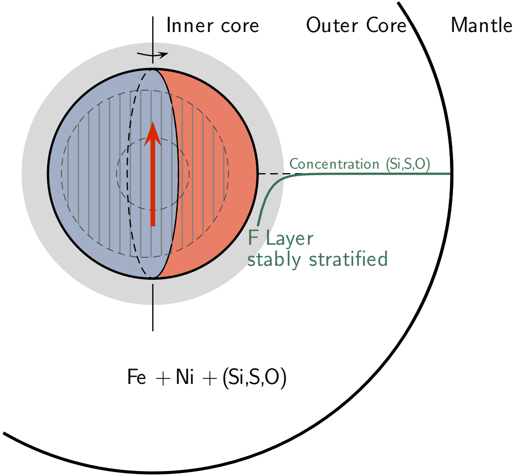

(fig. courtesy of R. Deguen)

- Seismic anisotropy (Morelli et al., 1986; Poupinet et al., 1983; Woodhouse et al., 1986).
- East–west dichotomy, possibly with sharp edges.
- A different innermost inner core.
- These observations call for one or more explanations.

Growth of the inner core with time

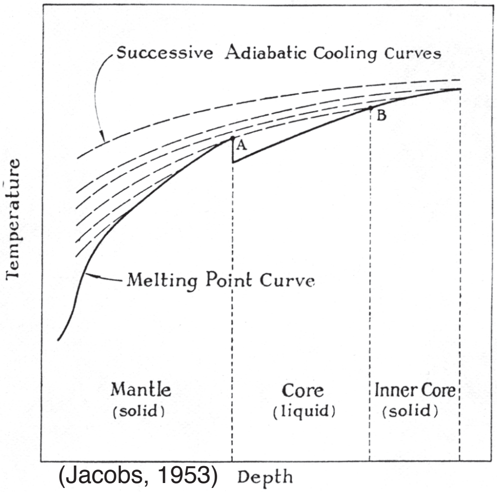

(Jacobs, 1953)

- Jacobs (1953) is the first to propose a progressive growth of the inner core.

- Energy balance of the core ⇒ inner core growth, evolution of temperature, etc. (e.g. Labrosse et al., 1997)
- Classically, temperature in the inner core is assumed to evolve by diffusion.

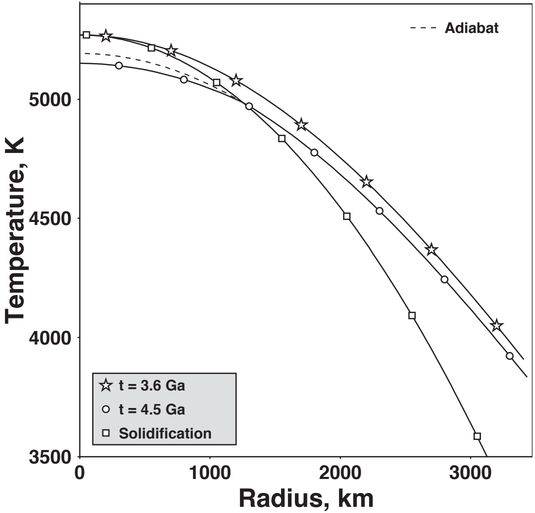

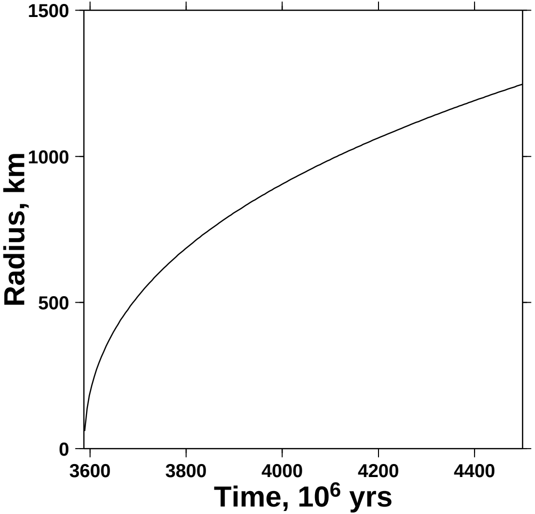

Formation of dendrites during crystallisation

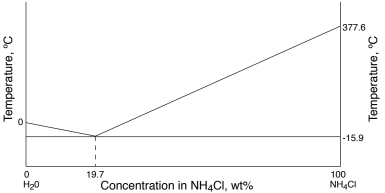

- Compositional convection in water driven by fractional crystallisation.
- Compositional plumes emerge from inter–dendrite space or chimneys.

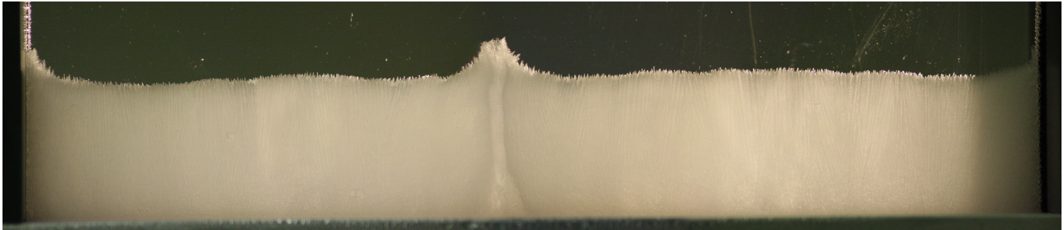

Dendrites and chimneys

NH_4Cl, pictures courtesy of R. Deguen

- Seen from the side

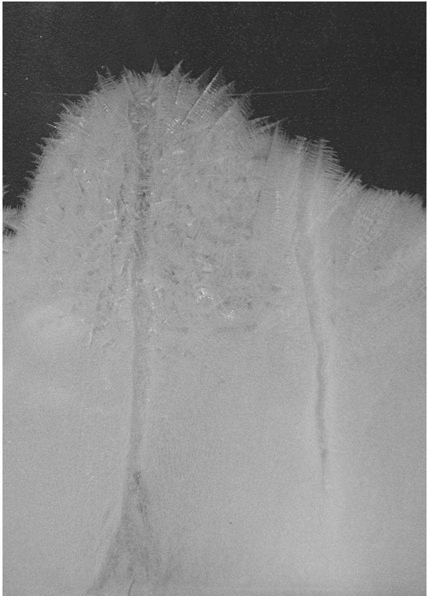

- Seen from above

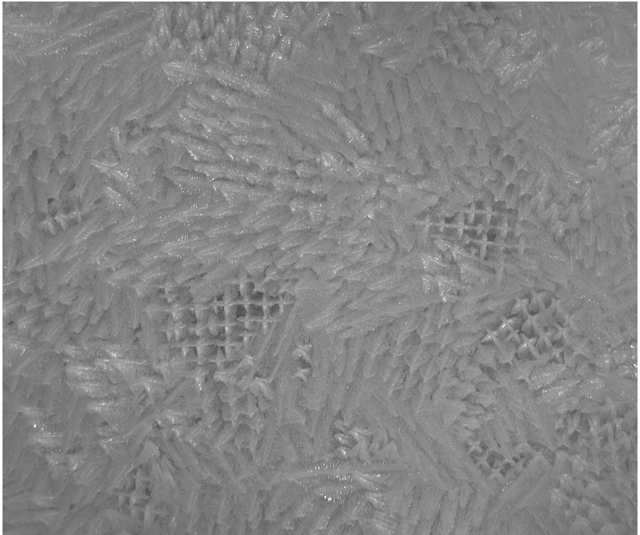

Anisotropy acquired during crystallisation
Bergman (1997)

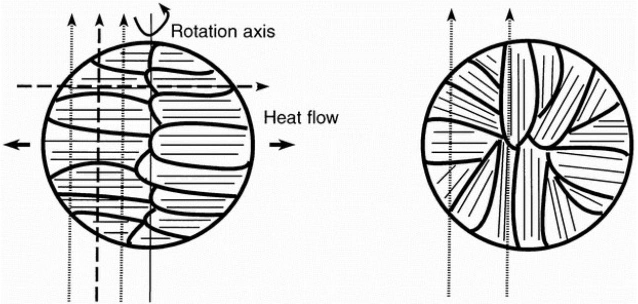

- Crystal growth in a specific orientation owing to the largest heat flow in the equatorial plane.
- May also be influenced by the local flow direction, as for sea ice (Bergman et al., 2002).
- Karato (1993) proposed that crystal growth influenced by the Lorentz force.
- Application to the inner core assuming HCP crystals.
- A strong toroidal magnetic field is necessary for this scenario.

Deformation induced by the Lorentz force

Karato (1993)

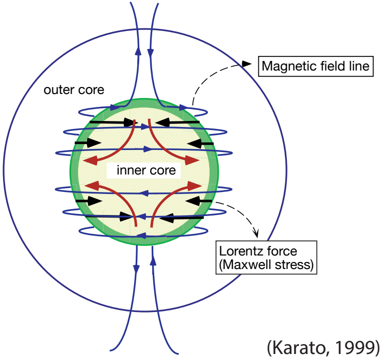

(Karato, 1999)

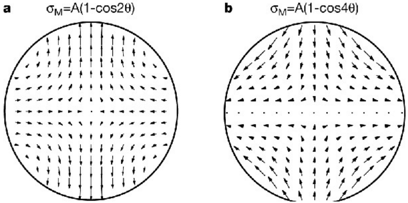

- Toroidal magnetic field causes a Maxwell stress on the inner core, computed as acting only on the surface.

$\Rightarrow$ flow in the inner core and development of LPO.

- But Buffett and Bloxham (2000) suggest that the flow should be too small to explain the observations.
- Buffett and Wenk (2001) propose the tangential Maxwell stress as driving force to produce deformation and LPO.

Viscous relaxation owing to differential growth
Yoshida et al. (1996)

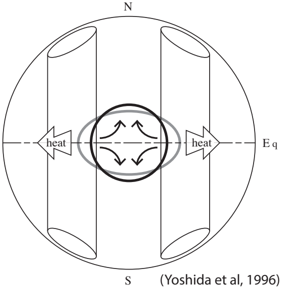

(Yoshida et al, 1996)

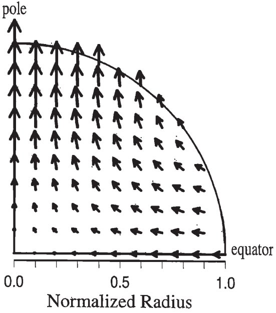

- Dynamics of the outer core dominated by rotation

$\Rightarrow$ heat transfer expected to be more efficient in the equator.

- Density difference between the solid and the liquid

$\Rightarrow$ flow in the inner core induced by the weight of topography.

- Flow in the solid can lead to lattice preferred orientation (LPO) and anisotropy.

Thermal convection in the inner core

Jeanloz and Wenk (1988) and Weber and Machetel (1992)

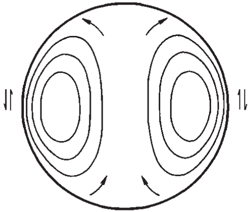

Fig. 1. Cross section through the inner core with streamlines illustrating the lowest mode that is unstable to convection [after Chandrasekhar, 1961]. Arrows schematically indicate the pattern of flow and the sense of shear in the outer, equatorial region.

- Early studies: convection driven by internal heating, which is likely negligible.
- Secular cooling could work similarly but it requires a very small thermal conductivity or a fast inner core growth (see below).

Convection driven by lateral variations of Joule heating
Takehiro (2011)

Lateral variations of the Joule heating $\Rightarrow$ baroclinic flow.

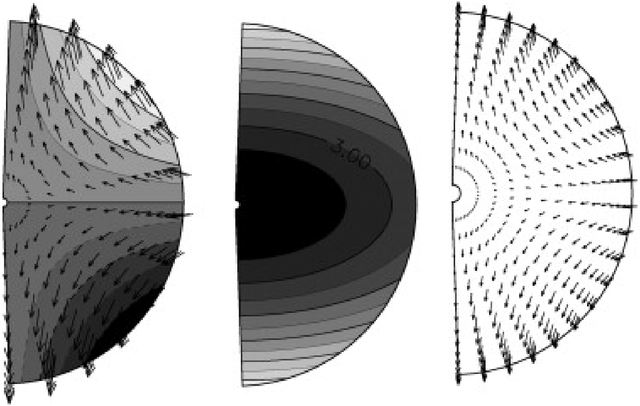

- Y_2^0 Toroidal field and current.
- Joule heating.
- Fluid flow.

Summary of the different scenarios

Texture can be acquired:

- Because of the crystallisation process.
- Because of a large scale flow:
  - owing to an external forcing (topography, Maxwell stress)
  - or convection.
- Convection from lateral variations of Joule heating happens without threshold on the Rayleigh number.
- Convection of the Rayleigh–Bénard style needs an unstable stratification.
- Whatever the mechanism, it is influenced by the base stratification and the boundary conditions.
- The stratification depends on the growth history of the inner core.

- The basic conductive state is influenced by the moving boundary at a Peclet number $Pe = u_{ic} r_{ic}/\kappa$.

Fast inner core growth,
low thermal conductivity,
large $dT_m/dT_{\rm ad}$

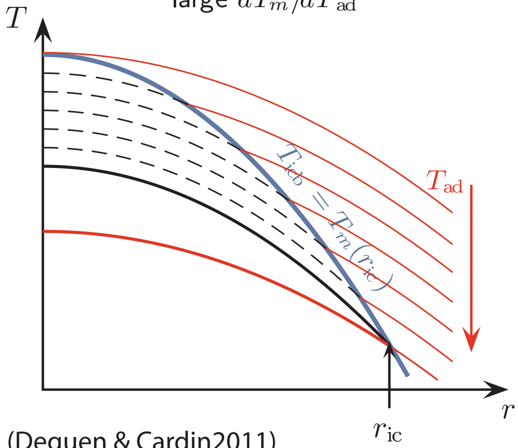

(Deguen & Cardin2011)

Slow inner core growth,
large thermal conductivity,
low $dT_m/dT_{\rm ad}$

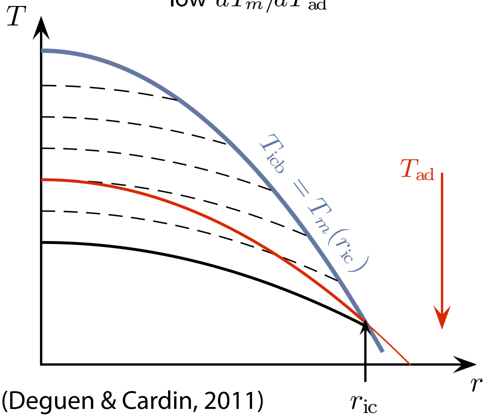

(Deguen & Cardin, 2011)

Approximate criterion for instability I

Deguen and Cardin (2011)

- Diffusion with a moving boundary

$$\frac{\partial T}{\partial t} = \kappa \boldsymbol{\nabla}^2 T \text{ and } T(r_{ic}(t)) = T_m(r_{ic}(t))$$

- Potentially unstable if

$$\left|\frac{\partial T}{\partial r}\right| > \left|\frac{\partial T_a}{\partial r}\right|$$

- Equation written for the super–isentropic temperature, $\theta = T - T_a$:

$$\frac{\partial \theta}{\partial t} = \kappa \boldsymbol{\nabla}^2 \theta + \underbrace{\kappa \boldsymbol{\nabla}^2 T_a - \frac{\partial T_a}{\partial t}}_{\text{effective heating, } S(t)}$$

- Effective heating can be approximated by

$$S(t) = \frac{\rho g' \gamma}{K_S} T_a \left[\left(\frac{\partial T_m}{\partial T_a} - 1 \right) \frac{1}{2} \frac{\mathrm{d} r_{ic}^2}{\mathrm{d} t} - 3\kappa \right]$$

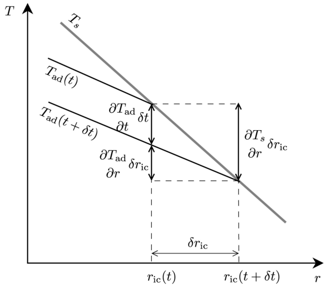

- Diffusion profile can become unstable if $S(t) > 0$:

$$\frac{\mathrm{d}\,r_{ic}^2}{\mathrm{d}t} > \frac{6\kappa}{\dfrac{\partial T_m}{\partial T_a} - 1}.$$

- Assume $r_{IC}(t) \propto \sqrt{t} \Rightarrow \dfrac{\mathrm{d}\,r_{ic}^2}{\mathrm{d}t} = r_{ic}^\star/\tau_{ic}$, with $r_{ic}^\star$ the present day radius of the inner core and τ_{ic} its age. Then, thermal stratification is unstable if

$$\tau_{ic} < \tau_\kappa \left(\frac{\partial T_m}{\partial T_a} - 1 \right) \text{ with } \tau_\kappa = \frac{r_{ic}^{\star 2}}{\kappa}$$

- Dimensionless control parameter:

$$\mathcal{T}_{ic} = \frac{r_{ic}^{\star 2}}{\kappa} \left(\frac{\partial T_m}{\partial T_a} - 1 \right)^{-1}$$

Quantitative assessment
Deguen and Cardin (2011)

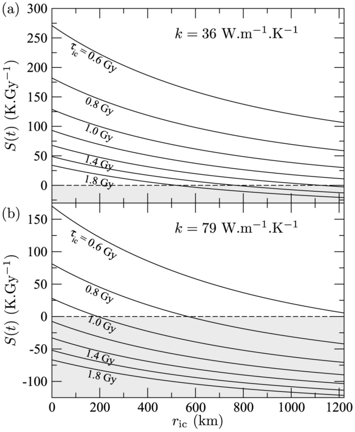

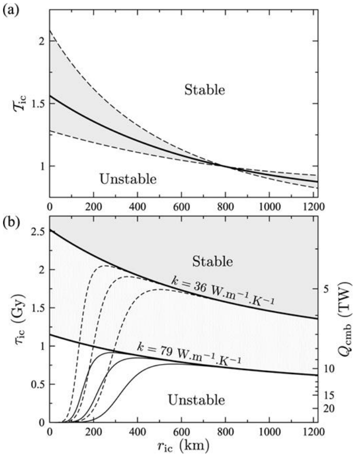

- Calculations done using a full thermal evolution model.
- Competition between growth speed of the inner core and diffusion.
- For a constant CMB heat flow, the inner core is most likely to convect early in its history.
- Current estimates of core conductivity (Gomi et al., 2013; Koker et al., 2012; Pozzo et al., 2012, e.g.), $k \geq 90\,\mathrm{W/m/K}$: thermal convection unlikely.

Convection with a non–penetrative boundary condition I

Deguen and Cardin (2011)

- Young inner core, small conductivity $\Rightarrow$ ongoing convection.

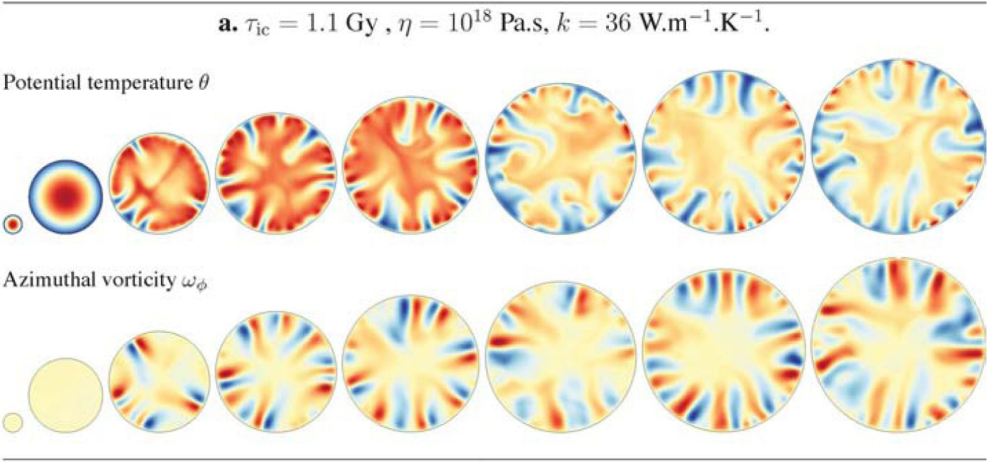

Convection with a non–penetrative boundary condition II
Deguen and Cardin (2011)

- Older inner core, small conductivity ⇒ convection during a part of the history. Could that be an explanation for the innermost inner core?

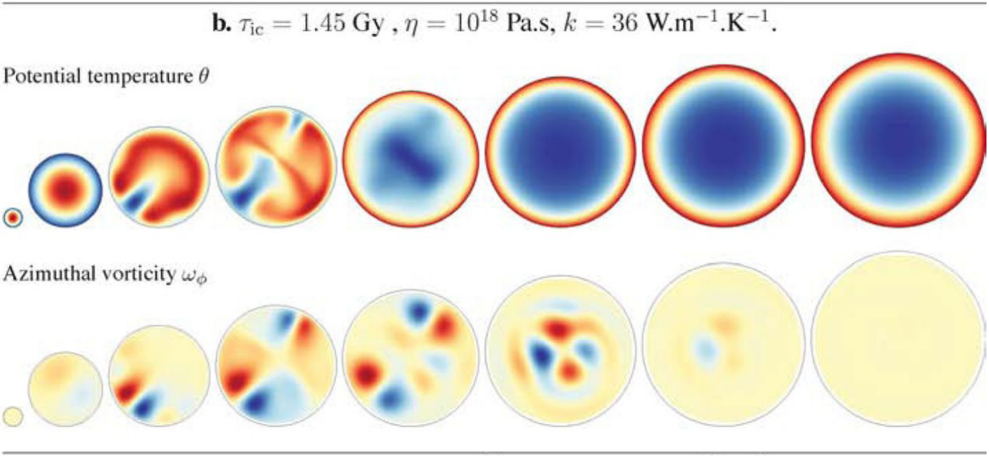

Convection with a phase change boundary condition
Alboussière et al. (2010) and Deguen et al. (2013)

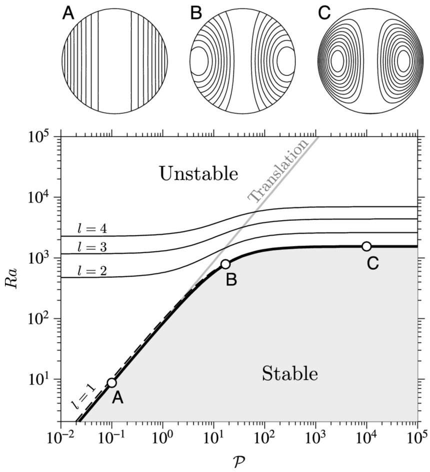

- The phase change BC first introduced

$$-\mathcal{P}(u_r - \dot{r}_{ic}) - 2\,\frac{\partial u_r}{\partial r} + p = 0$$

  with $\mathcal{P}$ the phase change number.
- Degree 1 convection at onset.
- Low values of $\mathcal{P}$ give the translation mode of convection.

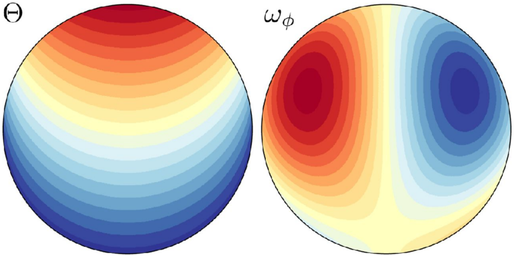

- See also Mizzon and Monnereau (2013).

Regime diagram
Deguen et al. (2013)

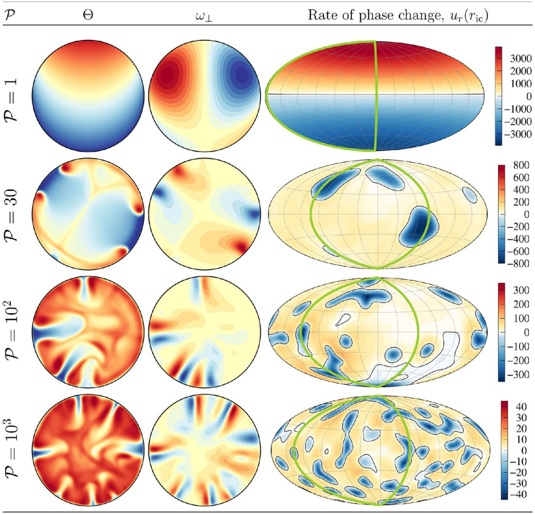

- Depending on the value of $\mathcal{P}$:
  - translation
  - plume convection
- Thermal convection still requires unstable stratification.

Compositional stratification

Gubbins et al. (2013) and Labrosse (2014)

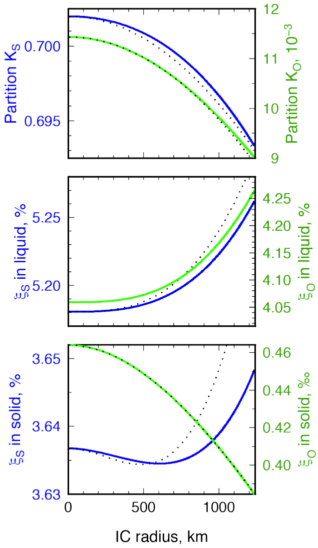

- Concentration of light element X in the solid and the liquid related by $C_X^s = P_X^{sl} C_X^l$
- $P_X^{sl} < 1 \Rightarrow C_X^l$ increases with time.
- Partition coefficient obtained from the temperature- and composition-dependent equilibrium condition

$$\mu_0^l + \lambda^l C^l + k_B T \ln(C^l) = \mu_0^s + \lambda^s C^s + k_B T \ln(C^s).$$

  Decrease of liquidus $\Rightarrow$ decrease of P_X^{sl} (Gubbins et al., 2013).
- Resulting evolution of mass fractions and corresponding partition coefficient shown on the figure.
- Leading order development (dotted lines):

$$\frac{\delta \xi_X^s}{\xi_{X0}^s} = -B_X r_{IC}^2 + A_X r_{IC}^3.$$

- O potentially destabilising, S starts destabilising and ends stabilising.

Resulting total buoyancy
Labrosse (2014)

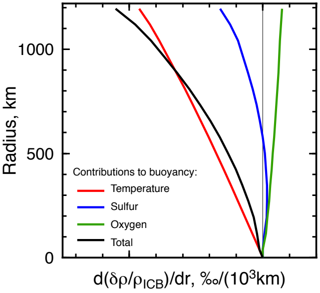

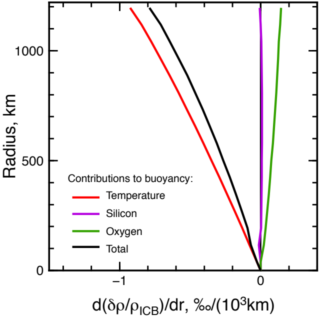

- Two compositional models considered (Gubbins et al., 2013): O and S or O and Si.
- Buoyancy computed as

$$\frac{\delta\rho(r)}{\rho_{ICB}} = -\,\alpha\left[T(r) - T_a(r)\right] + \sum \beta_i\left[\xi_i(r) - \xi_{if}\right]$$

- Suggests a stable stratification. Double–diffusive convection is still possible (see below).

Effect of stable stratification on Yoshida's scenario

Tectonic history of the Earth's inner core preserved in its seismic structure (2009)

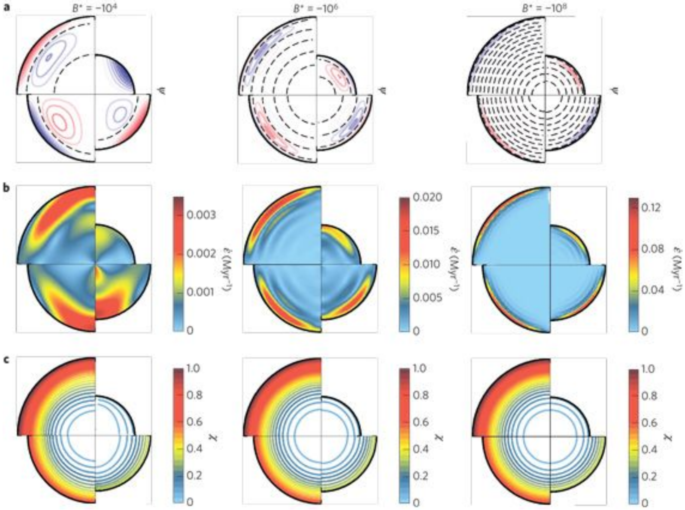

- Stream function (a), Strain rate (b) and composition (c)
- Increasing stability of the stratification (buoyancy number) leads to deformation restricted to a thinner outer shell.

- $Le = \kappa_T / \kappa_C \gg 1$.
- A vertically displaced fluid parcel equilibrates thermally faster than compositionally.
- It can raise even if the density is stably stratified.
- Translation mode independent from viscosity. Control parameters:

$$\mathcal{R}_\chi = \frac{\alpha_c \rho \Delta\chi}{\Delta\rho} \frac{r_{ic}^2}{\kappa \tau_\phi} = \frac{Ra_\chi}{\mathcal{P}}$$

$$\mathcal{B} = \frac{\alpha_T S_T}{\alpha_c S_c}$$

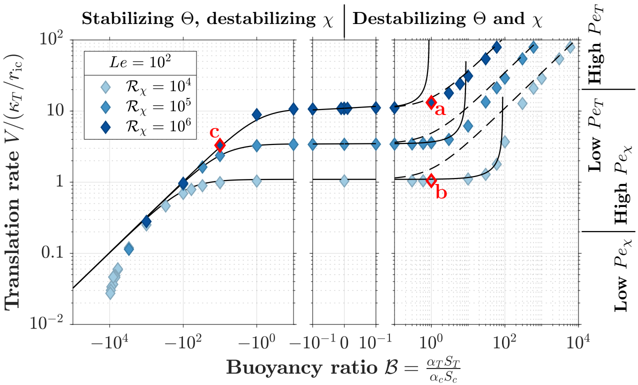

- Lines: approximate analytic translation velocity. Symbols: results from numerical models.
- Slow double–diffusive translation is possible even for a strongly stabilising temperature profile.

Double–diffusive translation of the inner core

Deguen et al. (2018)

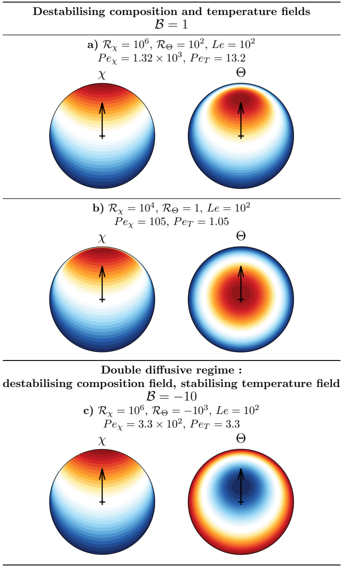

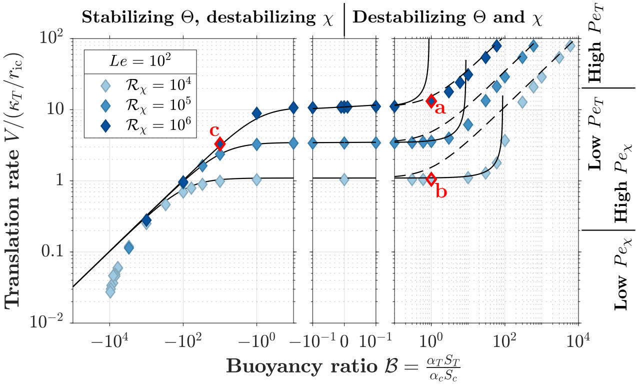

Effect of the phase change number

Deguen et al. (2018)

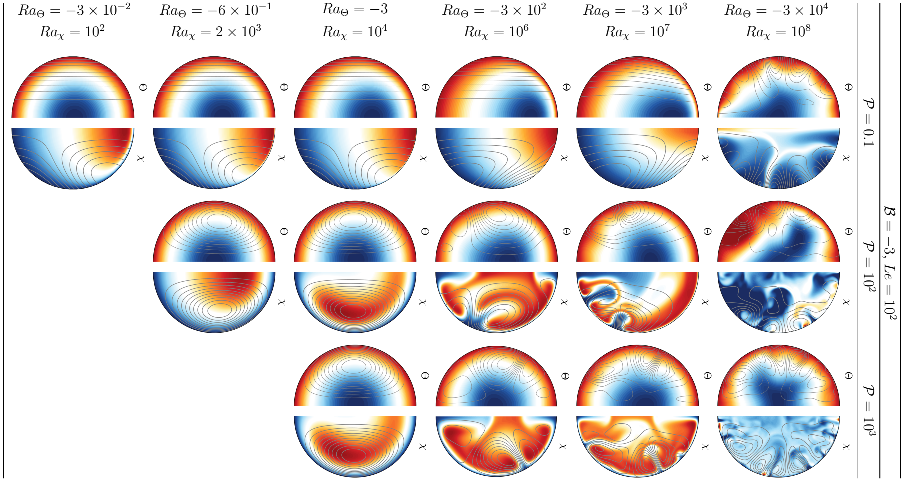

- Translation breaks down at large $\mathcal{P}$

Regime diagram

Deguen et al. (2018)

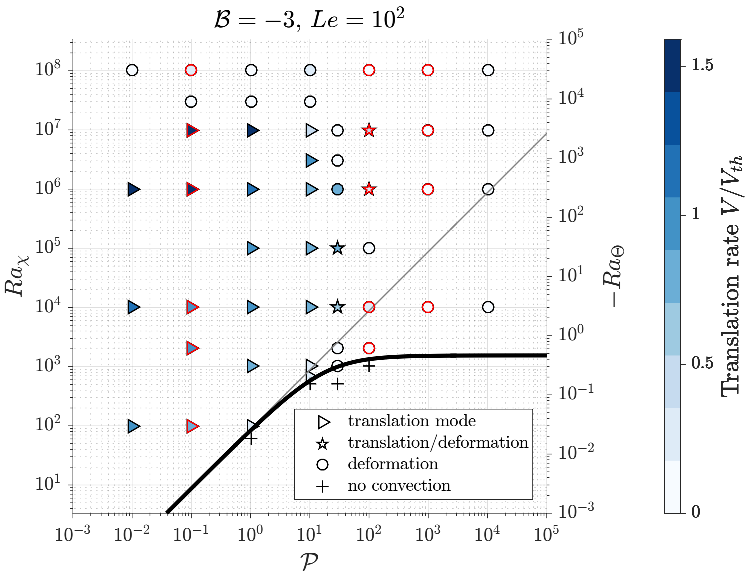

Summary on the dynamics of the inner core
Lasbleis and Deguen (2015)

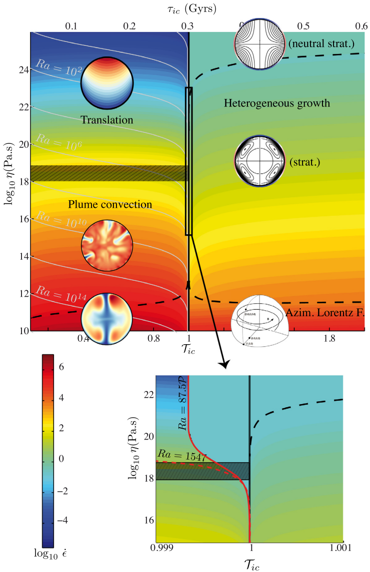

- Many possible scenarios for deformation of the inner core.
- Depending on the inner core age, temperature profile can be stably stratified or lead to convection.
- For stably stratified density distribution, double–diffusive convection still possible if the compositional stratification is unstable.
- Other scenarios must work against any stable stratification.
- No scenario seems able to explain all observations, in particular the large seismic anisotropy.

Conclusions

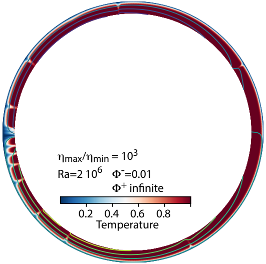

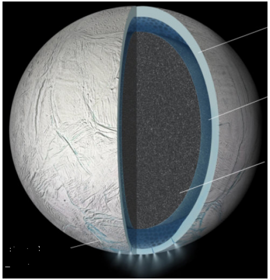

- Convection in solid shells of planets is a rich phenomenon with many complexities and many aspects yet to be understood.
- Key example: plate tectonics on Earth and not on other planets.
- Some aspects not covered in this lecture:
  - Two–phase flow. Key to understand volcanism and also the mushy regions at the interface with liquid layers (outer core, magma oceans).
  - History–dependent rheology: damage, anisotropic, grain-size dependent. Probably important for plate tectonics.
  - Effect of volatiles (H, C) and global cycles with the hydrosphere. Effect on rheology is expected.
- Boundary conditions are critical (e.g. Ishiwatari et al., 1994; Takehiro et al., 2002)! The phase change boundary condition considerably changes the dynamics and heat transfer.
- Many implications for the Early Earth but also icy satellites.

- Agrusta, R., A. Morison, S. Labrosse, R. Deguen, T. Alboussière, P. J. Tackley, and F. Dubuffet (2019). Mantle convection interacting with magma oceans. *Geophys. J. Int.* in press.
- Alboussière, T., R. Deguen, and M. Melzani (2010). Melting-induced stratification above the Earth's inner core due to convective translation. *Nature* **466**: 744–747.
- Bergman, M. I. (1997). Measurements of elastic anisotropy due to solidification texturing and the implications for the Earth's inner core. *Nature* **389**: 60–63.
- Bergman, M. I., D. M. Cole, and J. R. Jones (2002). Preferred crystal orientations due to melt convection during directional solidification. *J. Geophys. Res.* **107**: ECV 6–1–ECV 6–8.
- Buffett, B. A. and J. Bloxham (2000). Deformation of Earth's inner core by electromagnetic forces. *Geophys. Res. Lett.* **27**: 4001–4004.
- Buffett, B. A. and H.-R. Wenk (2001). Texturing of the Earth's inner core by Maxwell stresses. *Nature* **413**: 60–63.
- Deguen, R., T. Alboussière, and P. Cardin (2013). Thermal convection in Earth's inner core with phase change at its boundary. *Geophys. J. Int.* **194**: 1310–1334.
- Deguen, R., T. Alboussière, and S. Labrosse (2018). Double-diffusive translation of Earth's inner core. *Geophys. J. Int.* **214**: 88–107.

- Deguen, R. and P. Cardin (2011). Thermochemical convection in Earth's inner core. *Geophys. J. Int.* **187**: 1101–1118.
- Gomi, H., K. Ohta, K. Hirose, S. Labrosse, R. Caracas, M. J. Verstraete, and J. W. Hernlund (2013). The high conductivity of iron and thermal evolution of the Earth's Core. *Phys. Earth Planet. Inter.* **224**: 88–103.
- Gubbins, D., D. Alfè, and C. J. Davies (2013). Compositional instability of Earth's solid inner core. *Geophys. Res. Lett.* **40**: 1084–1088.
- Hernlund, J. W. and P. J. Tackley (2008). Modeling mantle convection in the spherical annulus. *Phys. Earth Planet. Inter.* **171**: 48–54.
- Ishiwatari, M., S.-I. Takehiro, and Y.-Y. Hayashi (1994). The effects of thermal conditions on the cell sizes of two-dimensional convection. *J. Fluid Mech.* **281**: 33–50.
- Jacobs, J. A. (1953). The Earth's inner core. *Nature* **172**: 297–298.
- Jeanloz, R. and H.-R. Wenk (1988). Convection and anisotropy of the inner core. *Geophys. Res. Lett.* **15**: 72–75.
- Karato, S. (1993). Inner core anisotropy due to the magnetic flied-induces preferred orientation of iron. *Science* **262**: 1708–1711.

- Koker, N. de, G. Steinle-Neumann, and V. Vlček (2012). Electrical resistivity and thermal conductivity of liquid Fe alloys at high P and T, and heat flux in Earth's core. *Proc. Nat. Acad. Sci. U.S.A.* **109**: 4070–4073.
- Labrosse, S. (2014). Thermal and compositional stratification of the inner core. *C. R. Geosciences* **346**: 119–129.
- Labrosse, S., J.-P. Poirier, and J.-L. Le Mouël (1997). On cooling of the Earth's Core. *Phys. Earth Planet. Inter.* **99**: 1–17.
- Labrosse, S., A. Morison, R. Deguen, and T. Alboussière (2018). Rayleigh-Bénard convection in a creeping solid with a phase change at either or both horizontal boundaries. *J. Fluid Mech.* **846**: 5–36.
- Lasbleis, M. and R. Deguen (2015). Building a regime diagram for the Earth's inner core. *Phys. Earth Planet. Inter.* **247**: 80–93.
- Mizzon, H. and M. Monnereau (2013). Implication of the lopsided growth for the viscosity of Earth's inner core. *Earth Planet. Sci. Lett.* **361**: 391–401.
- Morelli, A., A. M. Dziewonski, and J. H. Woodhouse (1986). Anisotropy of the inner core inferred from PKIKP travel times. *Geophys. Res. Lett.* **13**: 1545–1548.
- Morison, A., S. Labrosse, R. Deguen, and T. Alboussière (2019). Timescale of overturn in a magma ocean cumulate. *Earth Planet. Sci. Lett.* **516**: 25–36.

- Poupinet, G., R. Pillet, and A. Souriau (1983). Possible heterogeneity of the Earth's core deduced from PKIKP travel times. *Nature* **305**: 204–206.
- Pozzo, M., C. J. Davies, D. Gubbins, and D. Alfè (2012). Thermal and electrical conductivity of iron at Earth's core conditions. *Nature* **485**: 355–358.
- Tackley, P. J. (2008). Modelling compressible mantle convection with large viscosity contrasts in a three-dimensional spherical shell using the yin-yang grid. *Phys. Earth Planet. Inter.* **171**: 7–18.
- Takehiro, S.-I. (2011). Fluid motions induced by horizontally heterogeneous Joule heating in the Earth's inner core. *Phys. Earth Planet. Inter.* **184**: 134–142.
- Takehiro, S.-i., M. Ishiwatari, K. Nakajima, and Y.-Y. Hayashi (2002). Linear Stability of Thermal Convection in Rotating Systems with Fixed Heat Flux Boundaries. *Geophys. Astrophys. Fluid Dyn* **96**: 439–459.
- Tectonic history of the Earth's inner core preserved in its seismic structure (2009). *Nature Geosci* **2**: 419–422.
- Weber, P. and P. Machetel (1992). Convection within the inner-core and thermal implications. *Geophys. Res. Lett.* **19**: 2107–2110.
- Woodhouse, J. H., D. Giardini, and X.-D. Li (1986). Evidence for inner core anisotropy from free oscillations. *Geophys. Res. Lett.* **13**: 1549–1552.

Yoshida, S., I. Sumita, and M. Kumazawa (1996). Growth model of the inner core coupled with the outer core dynamics and the resulting elastic anisotropy. *J. Geophys. Res.* **101**: 28085–28103.